Siting Repowered Wind Turbines to Minimize Raptor Collisions at the Tres Vaqueros Wind Project, Contra Costa County, California

Draft Report to the East Bay Regional Park District

K. Shawn Smallwood and Lee Neher

28 April 2010

ABSTRACT: In support of a proposal to repower the Tres Vaqueros Wind Energy project, we related raptor flight observations to a digital elevation model (DEM) of the Vasco Caves Regional Preserve. Raptor flights were weighted by detection functions based on distance from the observer, by the volume of visible airspace within the maximum survey radius, by the degree of overlap in of the underlying location within all observation stations, and by the relative number of times surveys were performed at each station. Simple Fuzzy Logic models were developed to predict the locations of weighted golden eagle flights, red-tailed hawk and American kestrel hovering and kiting flights, and burrowing owl nest burrows. The highest likelihood surface – class 4 – generated from these models included mapped flying golden eagle observations 2.4 times other than expected, hovering and kiting red-tailed hawks 13 times other than expected, hovering and kiting American kestrels 12 times other than expected, and burrowing owl nest burrows 8 times other than expected. The likelihood surfaces were then extrapolated to the entire Tres Vaqueros project area. We also used geoprocessing steps to help identify ridge saddles, notches, and benches where wind turbine locations have been found to be more hazardous to raptors. Wind turbine siting should generally avoid the Fuzzy Logic likelihood surface class of 4 wherever it was mapped within the project area, and it should be cautious about installing wind turbines within the Fuzzy Logic likelihood surface class of 3.

INTRODUCTION

In recent years, wind power generation in the Altamont Pass Wind Resource Area (APWRA) annually provided about 700 gigawatt-hours (GWH) of renewable energy to California but also while causing the deaths of an estimated 2,230 raptors and 9,300 total birds per year (Smallwood and Karas 2009). Given the poor success of mitigation measures applied to the old-generation wind turbines, and given the substantial reductions in avian fatality rates at a repowered wind project in the APWRA (Diablo Winds), repowering the nearly 5,000 old-generation wind turbines to a much smaller number of modern wind turbines was recommended by Smallwood and Karas (2009). Furthermore, modern wind turbines operate at higher capacity factors than the APWRA's deteriorating, old-generation wind turbines, and so can generate much more electricity. This increased power generation can be balanced against even fewer avian fatalities by carefully siting the new wind turbines to avoid portions of the landscape that are more intensively used by raptors (and other birds), and more importantly, that are more frequently associated with certain behaviors thought to increase a bird's vulnerability to wind turbine collision.

Wind turbine siting to minimize avian collision hazard requires an understanding of how birds use the airspace over the landscape where new wind turbines are proposed or planned. This understanding can come from monitoring of bird activity and specific flight behaviors under various wind conditions and landscape settings, and by relating utilization rates and flight behaviors to fatality rates (Smallwood et al. 2009b,c). In the 543-ha Vasco Caves Regional Preserve, Smallwood et al. (2009b,c) monitored raptors from 15 observation stations for 774 hours total from June 2006 through September 2007. These observation data can be related to a digital elevation model (DEM) to derive predictive models of locations where raptors more often fly or perform certain behaviors. The predictive models can then be extrapolated to adjacent areas where new wind turbines are planned.

Bird monitoring in Vasco Caves Regional Preserve generally followed guidelines recommended by Gauthreaux (1996), Anderson et al. (1999), U.S. Fish and Wildlife Service (2003), and the California Energy Commission and California Department of Fish and Game (CEC & CDFG 2007). However, even though these guidelines have been applied many times in California and across the USA, no effort was made to adjust utilization rates for potentially substantial biases in use and interpretation of rates of utilization and behaviors. When relating bird observations to a DEM, interpretation of flight patterns can be confounded by relationships between bird detection rates and (1) distance of the bird from the observer, (2) the airspace visible from each observation station, and (3) duration of the observation session. For most species, detection rates should be expected to decline with increasing distance from the observer, decreasing visible airspace within the maximum survey radius due to obstructing hills and slopes, and increasing session duration as observers lose their concentration. The bias from session duration should not have been a problem for the observation data collected in Vasco Caves Regional Preserve because all sessions were of equal duration (1 hour), but the maximum survey radius of 600 m and the variation in complexity of terrain among observation stations provided ample opportunity for detection rates to vary for reasons other than decisions made by raptors about where to fly.

Based on newly available LIDAR data, we developed a new, more resolute DEM compared to Smallwood et al. (2009c). The new DEM has a 2-foot grid cell resolution instead of the 10-meter resolution used previously (Figure 1), though we used a 10-foot grid cell resolution when analyzing bird utilization data because the accuracy of the bird data did not warrant 2-foot resolution. We developed map-based predictive models of where raptors more often fly and perform specific hazardous behaviors, and we extended these models to the proposed Tres Vaqueros repowering project area to assist an effort to carefully site new wind turbines at locations intended to cause the least harm to wildlife while also serving the power generation objectives of the project owner. We also quantified biases in the observation data caused by distance from the observer and variation in visible air space among observation stations, and we adjusted our observation data for these biases when developing predictive models. Our specific study objectives were the following:

1. Develop predictive models of raptor flights and flight behaviors that relate to wind turbine collision hazard;

2. Extend map-based model predictions to the Tres Vaqueros project area to assist with planning exact wind turbine locations to minimize raptor collisions; and,

3. Quantify and adjust for biases in raptor detection rates due to distance from the observer and variation in visible airspace among observation stations.

METHODS

Study Site

APWRA.--The Altamont Pass Wind Resource Area encompasses about 165 km^2 (16,500 ha) of ridges and hills generally extending northwest to southeast in eastern Alameda and southeastern Contra Costa Counties, California. Located in the Inner Coast Range geomorphic province and bordering the Central Valley province, slopes are steep above intermittent streams, springs, and stock ponds. Elevations range 78 m to 470 m above mean sea level. Slopes are covered mostly by non-native, annual grasses, which grow mostly during January through March and are dead or dormant by June. Cattle grazers hold most of the land, leasing out wind energy rights to wind power companies. Wind turbines in the APWRA are arranged in rows of 2 to 62 turbines, typically along ridge crests (i.e., peaks of the ridge features) and ridgelines extending down toward ephemeral streams. Wind turbine rows also occupy slopes, valleys, and hill peaks, and all operate in winds from any direction, although most winds originate from the southwest or northwest. Old-generation wind turbine models are listed in Smallwood and Thelander (2008).

Tres Vaqueros.—The proposed repowering project site for Tres Vaqueros Windfarms LLC (Tres Vaqueros) is located within the northern portion of the APWRA, where elevations range 70 m to 300 m. The site is about 6 km southwest of Byron. The land encompassed by Tres Vaqueros includes a portion of the 2,983.35 acre Vasco Caves Regional Preserve, which is owned and managed by the East Bay Regional Park District (EBRPD) and a portion of the Los Vaqueros Reservoir watershed, which is owned and operated by the Contra Costa Water District (CCWD). However, no wind turbines are currently situated on CCWD land. Wind right ownership is complex. Blackhawk Nunn Partners and Vaquero Farms, Inc. retain wind rights to all of the land encompassed by Tres Vaqueros Windfarms LLC except for a 249.7 ha parcel within Vasco Caves Regional Preserve. The EBRPD retains the wind rights over this parcel, known as Souza 1. Pattern Energy owns the 86 330-KW Howden wind turbine addresses on Tres Vaqueros and has wind leases with EBRPD, Blackhawk Nunn Partners and Vaquero Farms, Inc. The original total rated capacity of the project was 28.8 MW, but only 25 MW were operational at any level between 2000 and 2008.

Utilization data

Raptor flights.—B. Karas, H. Snively, and S. Smallwood collected bird utilization data from 15 observation stations weekly from June 2006 through September 2007, totaling 774 1-hour sessions (Smallwood et al. 2009b). Birds were recorded out to 600 m from each station. Birds recorded during these sessions were also mapped onto hand-held hard-copy maps depicting aerial images of the area under observation and including prominent features and blue lines highlighting ridge crests. Observers wrote symbols onto the maps where they estimated raptors

and corvids were located at one-minute intervals, totaling 7,699 recorded observations. Mapped locations were then digitized as point features in ArcMap GIS layered onto a digital elevation model (DEM).

Bird attribute data were recorded into digital audio recorders and later transcribed to electronic spreadsheets. Attributes included species, number of individuals, flight behavior if flying, perch structure if perching, and height above ground. We also recorded interactions with other birds, and the number of minutes into the session. At the start of each session and at 15-min intervals we recorded temperature, wind speed, and wind direction.

Burrowing owls.—J. Barclay and L. Harmon searched for burrowing owls and their nest burrows from 33 observation points in 2006 and 39 points in 2007, using 10 x 40 binoculars and a 25 x 60 spotting scope from both inside and outside an automobile. They performed 15 surveys (54 hours) from 24 May to 2 August 2006, and 11 surveys (44 hours) from 3 April to 27 June 2007. In both years, 11 surveys were initiated during morning, generally spanning 08:00 hours to 13:00 hours. Nest burrows had a breeding pair in attendance during repeat surveys. To represent nest productivity, the maximum number of emergent juveniles between 2 and 4 weeks old was recorded. Burrowing owl burrows were characterized as point features in ArcMap GIS and layered onto our DEM of the study area. The analytical grid for the burrowing owl burrow model development consisted of 582,068 grid cells, which were within the property boundaries of the original Vasco Caves parcel and the Souza parcel.

Digital Elevation Model

We utilized two separate digital elevation model (DEM) grids for this project. The majority of geoprocessing tasks were performed using a 10 foot cell size DEM obtained from Contra Costa County. This data set was produced using Lidar data and ARC TIN software by Mapcon Mapping Inc. during 2007-2008. We also obtained 2 foot contour interval vector GIS data from Contra Costa County and produced by the same contractor. We then created a 2 foot DEM from the contours using ESRI software. The 2 foot DEM was used for slope and aspect modeling.

All derived parameters were calculated for the entire EBRPD property area, plus an aggregated 2,000 foot buffer (609 m) around 15 bird observation points, to ensure that all bird observations would be covered. The aggregated 609-m buffer served as our mask for analyzing previously collected bird data against the higher resolution DEM. The 609-m radius was converted to a 2,000 foot radius and an additional 200 feet was added to buffer modeling data for geoprocessing.

Within the Tres Vaqueros project area, we limited (masked) statistical analyses to data within the areas searched for raptors and corvids. The resulting analytical grid was composed of 908,297 10x10-foot cells, each cell assigned a unique membership number. The analytical grid was used to develop and test predictive models, which were later projected across the 147,073,509 two foot grid cells composing the EBRPD buffered area and the 5,460,000 ten foot grid cell size expanded area grid.

Slope Attributes

The same geoprocessing steps were used to characterize slope attributes as reported in Smallwood and Neher (2004, 2009) and Smallwood et al. (2009a,c), but this time we refined some steps to differentiate grid cells between ridge-like (convex) and valley-like (concave) tendencies. We used the Curvature function in the Spatial Analysis extension of ArcGIS 9.2 to calculate the curvature of a surface at each cell centroid. A positive curvature indicated the surface was upwardly convex at that cell, a negative curvature indicated the surface was upwardly concave, and a value of zero indicated the cell surface was flat. The curvature data (-51 to 38) were classified using the Natural Breaks (Jenks) function with 3 classes of curvature – convex, concave and mid-range. The break values were visually adjusted to minimize the size of the mid-range class. We used a series of geoprocessing steps called 'expand,' 'shrink,' and 'region group,' as well as 'majority filter tools' to enhance the primary slope curvature trend of a location. The result was a surface almost exclusively defined as either convex or concave (Figure 2). The convex surface areas consisted primarily of ridge crests and peaks, hereafter referred to as ridges, and the concave surface areas consisted primarily of valleys, ravines, ridge saddles and basins, hereafter referred to as valleys.

Line features representing the estimated average centers of ridge crests and valley bottoms (Figure 3) were derived from the following steps. ESRI's Flow direction function was used to create a flow direction from each cell to its steepest down slope neighbor, and then the Flow accumulation function was used to create a grid of accumulated flow through each cell by accumulating the weight of all cells flowing into each down slope cell. A valley started where 50 upslope cells had contributed to it in the Flow accumulation function, and a ridge started where 55 cells contributed to it. The flow direction and flow accumulation functions were applied to the ridges by multiplying the DEM by -2 to reverse the flow. Line features that represented ridges and valley bottoms were derived from ESRI's gridline and thin functions, which feed a line through the centers of the cells composing the valley or ridge. Thinning put the line through the centers of groups of cells ≥40 in the case of valleys.

The two foot slope analysis grid was used to create polygons with a relatively gentle slope. A Standard Deviation classification was used to identify areas with < 7.4 % slope. These areas were then converted to polygons and intersected with the ridge/valley lines to determine polygons associated with either ridge or valley descriptions. The borders of these polygons were converted to lines and combined with the ridge/valley line datasets, respectively, and polygons in valley features were termed *valley polygons* and polygons on ridge tops were termed *ridge polygons* (Figure 3).

Horizontal distances (m) were then measured between each DEM grid cell and the nearest valley bottom boundary (in the valley line combined data set) and the nearest ridge top boundary or ridgeline (in the ridgeline combined data set), referred to as *distance to valley* and *distance to ridge*, respectively. These distances were measured from the DEM grid cell to the closest grid cell of a valley bottom or ridgeline, respectively, not including vertical differences in position. The *total slope distance* was the sum of *distance to valley* and *distance to ridge*, and expressed the size of the slope. The DEM grid cell's position in the slope was also expressed as the ratio of

distance to valley and *distance to ridge*, referred to as the *distance ratio*. This expression of the grid cell's position on the slope removed the size of the slope as a factor.

The vertical differences between each DEM grid cell and the nearest valley bottom boundary and nearest ridge top boundary or ridgeline were referred to as *elevation difference*, and this measure also expressed the size of the slope. In addition to the trend in slope grade at each DEM grid cell, the *gross slope* was measured as the ratio of *elevation difference* and *total slope distance*. The DEM grid cell's position on the slope was also expressed as the ratio of the elevation differences between the grid cell and the nearest valley and between the grid cell and the nearest ridge, referred to as *elevation ratio*. Additionally, we measured the grid cell's position on the slope as the average of the percentage distance and the percentage elevation to the ridge top. This mean percentage was named *percent up slope* and provided a more robust expression of the grid cell's position on the slope (Figure 4).

Percent up slope did not distinguish a grid cell's position between slopes on large hills versus medium or small-sized hills, so we expressed the local topographic influence of the feature where each cell was located, where *hill size* was the elevation difference between the nearest valley bottom polygon and nearest prominent ridge top polygon (Figure 5).

Each DEM grid cell was classified by *aspect* according to whether it faced north, northeast, east, southeast, south, southwest, west, northwest, or if it was on flat terrain. Each grid cell was also categorized as to whether its center on the landscape was windward, leeward or perpendicular to the prevailing southwest and northwest wind directions as recorded during the behavior observation sessions.

Steps to identify saddles, notches, and benches

Because a growing body of evidence has linked disproportionate numbers of raptor fatalities to wind turbines located on aspects of the landscape that are lower than immediately surrounding terrain or that represent sudden changes in elevation, we made a special effort to identify ridge saddles, notches in ridges, and benches of slopes, which are where ridge features emerge from hill slopes that extend above the emerging ridge. These types of locations are where winds often compress by the landscape to create stronger force, and where raptors typically cross hilly terrain or spend more time to forage for prey items. Compared to surrounding terrain, these types of features are often relatively flatter or shallower in slope and sometimes include lower elevations (e.g., saddles). We used geoprocessing steps to provide some objectively to the identification of these features, but we also had to also use judgment because conditions varied widely in how such features were formed and situated.

We used the same procedures as used in the ridge/valley selection. The two foot slope analysis grid was used to create polygons with a relative gentle slope. A Standard Deviation classification was used to identify areas with < 7.4 % slope. These areas were then converted to polygons. Those polygons not associated with ridge or valley polygons were examined manually. Where these polygons were visually associated with saddle and or step features, they were identified as polygons representing saddles, notches, or benches. We also examined maps depicting contours of the variable *percent up slope*, because these contours readily revealed

sudden breaks in slope typical of saddles, notches, and benches, which we also represented with polygons.

Visible and Hidden Volumes of Surveyed Airspace

At each 10x10 foot grid cell, we extruded volumes of airspace upward at 10-foot increments to a 460-foot (140.2 m) ceiling above the observer at each observation station, and each cube of airspace was classified whether it was visible or hidden from each observation station by line of sight. Cubic volumes of air space were each 1000 feet^3 (28.31 m^3). Visible versus hidden volumes of airspace were summed within 20 equidistant radial bands extending laterally from each observation station, each band 100 feet (30.48 m) farther from the last and the outer survey boundary 2000 feet (609 m) from the observer.

We summed the first observations of raptors recorded during utilization surveys, and converted the sums to detection rates. The most basic detection rate was number of observations per hour (each session was an hour). We also calculated a detection rate as the number of observations per hour per km^3 of visible airspace within each sequentially larger outer survey boundary, where boundaries were increased in 100-foot radial increments. The detection rates calculated within sequentially larger boundaries were spatially correlated because the numbers of birds within inner radial bands contributed cumulatively to the numbers also counted within outer radial bands. To remove the effect of this spatial correlation, we also calculated a detection rate as the number of observations per hour per km^3 of visible airspace within each sequential, 100-foot radial band extending from the observer, for which the numbers of observations closer to the observer did not contribute to the numbers observed within each specific band, i.e., the counts within each radial band were independent rather than cumulative. In either case, we compared detection rates to distance intervals from the observer and fit regression models to the patterns in the data.

Species-specific detection rates (first observations/km^3/hour) were predicted for all grid cells within the masked study area, based on their distances from observation stations within 609 m. Each predicted detection rate was divided by the maximum possible – the rate estimated within 100 feet of the observation station. Thus, each grid cell was assigned a proportional weighting of detection likelihood relative to the nearest radial band to the observer. These proportions were summed when a grid cell was within 609 m of >1 observation station, e.g., a grid cell with a detection weighting (D) of 0.18 from station 9 and a weighting of 0.07 from station 13 would be given a summed weighting of 0.25. Grid cells were further weighted (W) by the relative number of observation sessions per station (S) where the number of sessions at a station was divided by the maximum number achieved among all the stations:

$$W_i = \frac{\sum D_i}{D_{MAX}} \times \frac{S_i}{S_{MAX}} \quad ,$$

where the *i*th grid cell could range in weightings from 0 to 1.

Associations between bird utilization and slope attributes

We characterized the location of each raptor by aspect, slope, rate of change in slope, direction of change in slope, and elevation. These variables were also used to generate raster layers of the study area, one raster expressing the aspect of the corresponding slope (hereafter referred to as *aspect*), and the other expressing whether the landscape feature was tending toward convex versus concave orientation. These features were defined using geoprocessing.

Log_{10} and natural log transformations were used to better fit normal distributions, and then chi-square tests for association and principal components analysis (PCA) were used to further understand how the variables related to raptor locations and to each other. To minimize the effects of confounding, no more than one predictor variable was selected from each principle component for any model developed to classify grid cells according to whether they associated with raptor locations.

We used fuzzy logic (FL) modeling (Tanaka 1997, Kainz 2004) to predict the likelihood each grid cell would be used by golden eagle, red-tailed hawk, American kestrel, and burrowing owl. FL likelihood surfaces were first created by each selected predictor variable. For each predictor variable, we calculated the mean, standard deviation, and standard error among the grid cells where each targeted bird species was observed during standard observation sessions. These statistics formed the basis from which we assigned FL membership to grid cells. Depending on the pattern in the data, we assigned FL membership values of 1 whenever the value of the predictor variable was within a certain prescribed distance in value from the mean, oftentimes within 1 SD, but sometimes within 1 or 2 SE. FL membership values of 1 expressed our confidence that grid cells with the corresponding value range for the predictor variable are likely to be visited by the target species. FL membership values of 0 were assigned to grid cells that were far from the mean value, usually defined by prescribed distances from the mean such as >2 SD from the mean. FL membership values of 0 expressed our confidence that grid cells with the corresponding value range for the predictor variable are unlikely to be visited by the target species. All other grid cells were assigned FL membership values according to the following formulae, assuming that the likelihood of occurrence of each species will grade gradually rather than abruptly across grid cells that vary in value of the predictor variable (Y):

$$0.5 \times (1 - \cos(\pi \times (Y - V_c) \div (V_f - V_c))) \text{ below the mean}$$
$$0.5 \times (1 + \cos(\pi \times (Y - V_c) \div (V_f - V_c))) \text{ above the mean,}$$

where V_c represented the variance term (SD or SE) closer to the mean and V_f represented the variance term farther from the mean.

FL likelihood values were then summed across predictor variables contributing to a species-specific model, and natural breaks were used to divide the summed values into 4 classes: 1 represented the suite of grid cells including fewer bird observations other than expected, 2 represented the suite of grid cells including about equal or slightly greater than equal bird observations other than expected, 3 represented the suite of grid cells including more bird observations other than expected, and 4 represented the suite of grid cells including substantially more bird observations other than expected. The performance of each model was assessed by the

magnitude of the ratio of the observed number to the expected number of observations occurring within the suite of conditions specified by each FL surface class, where consideration was also given to fewer numbers of predictor variables and smaller portions of the study area contributing to the ratios in surface classes 2, 3, and 4. FL surface models were later projected across the entire Tres Vaqueros project area. We also extended our mapping of special landscape features to the entire Tres Vaqueros project area.

RESULTS

Bird detection rates

The volume of airspace that was visible from the observation station decreased with increasing distance from the observer in Vasco Caves Regional Preserve, though the change in the percentage of airspace that was visible also varied considerable among stations (Figure 6). The visible volume of airspace over unobstructed, flat terrain within a 600 m radius and 140 m ceiling would be 158,336,269.7 m^3, or 0.1583 km^3, but over the complex terrain of Vasco Caves Regional Preserve it ranged from 0.1299 to 0.1919 km^3 (Figure 7), due to hills rising above observation stations and valleys descending below. Relative to the airspace that would be expected of flat terrain, this variation in visible airspace due to complex terrain translated into an initial reduction of visible airspace with increasing distance from the observer to about 600 feet away, followed by a gradual increase until the volumes of airspace observable was about the same at 2,000 feet away. To account for the variation in visible airspace among stations, we calculated avian utilization rates as the number of birds/hr/km^3 of visible airspace within a 140 m ceiling.

The mean number of first detections per hour increased with increasing distance from the observer (Figure 8), but not at the exponential rates that would be expected of spatial distributions that were unrelated to the locations of observation stations (bottom right graph of Figure 8). Adjusted for the volume of visible airspace, the mean number of first detections per hour decreased with increasing distance from the observer (Figure 9, Table 1). Assuming birds were distributed randomly with respect to the observation stations and that detection accuracy was greatest within the closest 100 - 200 feet of airspace from the observer, then detection rates declined steeply with increasing distance from the observer (see horizontal dashed lines in Figure 9). An interesting exception to this pattern was for burrowing owls, which were most detectable either at 200 feet or between 700 and 800 feet from the observer, but the pattern of declining detection rates resumed for burrowing owl beyond 800 feet (Figure 9).

Detection rates within specific radial bands from the observer varied inter-specifically (Figure 10), revealing lower detection rates of some species nearby the observer, peaks in detection rates of some species at specific distances from the observer, and increasingly greater detection rates with distance for some species such as red-tailed hawk (Figure 10). However, again assuming birds were unaffected by the locations of observation stations, detection rates were increasingly lower than expected rates as the distance from the observer increased (see solid line in bottom right graph in Figure 10). Adjusted for the volume of visible airspace within specific radial bands, the mean number of first detections per hour again decreased with increasing distance from the observer (Figure 11, Table 2), though decreases were more rapid and nadir's were

reached closer than when detection rates were adjusted for the cumulative volume of visible airspace with increasing distance from the observer (Figure 9).

For perspective, we compared detection rates within radial bands and cumulatively with increasing distance from the observer (Figure 12). Figure 12 illustrates how much faster detection rates decline with increasing distance when detection rates are restricted to within radial bands from the observer, even for large-bodied species such as golden eagle. The number of birds seen nearby dominates detection rates attributed to increasingly greater distances from the observer.

Table 1. First detections/hr/km3 visible airspace within circle regressed on distance from observer.

		Model parameters				
Species/Group	**Model**	**a**	**b**	**r^2**	**SE**	**P**
Golden eagle	Power	12.6915	-0.7430	0.97	0.10	0.001
Red-tailed hawk	Power	90.0736	-0.6041	0.96	0.10	0.001
Turkey vulture	Power	66.4367	-0.7159	0.97	0.11	0.001
Northern harrier	Logarithmic	11.0526	-3.2695	0.95	0.63	0.001
Prairie falcon	Power	21.8581	-1.1817	0.98	0.14	0.001
American kestrel	Power	75.5038	-1.0143	0.94	0.21	0.001
Burrowing owl	None					
Raptors	Power	281.1493	-0.7349	0.97	0.10	0.001
Common raven	Power	306.0222	-0.7777	0.97	0.12	0.001

Table 2. First detections/hr/km3 of visible airspace within radial bands regressed on number of 30.75-m radial bands from the observer.

		Model parameters				
Species/Group	**Model**	**a**	**b**	**r^2**	**SE**	**P**
Golden eagle	Inverse	0.3842	10.5260	0.88	0.91	0.001
Red-tailed hawk	Power	86.3666	-0.7585	0.91	0.20	0.001
Turkey vulture	Power	65.3069	-0.9403	0.88	0.29	0.001
Northern harrier	Logarithmic	10.4761	-3.6200	0.87	1.19	0.001
Prairie falcon	Inverse	-1.1380	16.9745	0.96	0.83	0.001
American kestrel	Inverse	-1.6516	54.0601	0.95	2.84	0.001
Burrowing owl	None					
Raptors	Power	295.2248	-0.9994	0.96	0.18	0.001
Common raven	Power	369.0675	-1.1663	0.91	0.31	0.001

Landscape used to develop predictive models

Principal components analysis, using a correlation matrix and varimax rotation, explained 65% of the variation in predictor variables measured among the grid cells in Vasco Caves (Table 3). Component 1 can be interpreted as position on the slope. Component 2 can be interpreted as the slope's rate of change, i.e., steepness. Component 3 can be interpreted as the slope's orientation

and size. Only one variable with a high loading was used from each component for subsequent predictive model development, though all variables were tested for relationships with avian activity levels.

Table 3. Principal Components following varimax rotation in PCA, showing only those rotated factor loadings >0.1.

Variable	Component 1 Position on slope	Component 2 Slope steepness	Component 3 Slope orientation & size
ln Distance ratio	0.982		
ln Elevation ratio	0.939		
$\log_{10}$ Distance to valley	0.887	0.243	
$\log_{10}$ Distance to ridge	-0.846	0.275	
Elevation	0.436		
Elevation difference		0.944	-0.120
Gross slope		0.835	0.206
$\log_{10}$ Total slope distance		0.622	-0.560
Slope (percentage)	0.107	0.607	0.369
Aspect		0.127	0.722
Percent up slope	0.175		-0.216
Percent of variance	**32.6**	**22.7**	**10.0**

Topographic associations

The grid cell's position as a percentage up slope, represented by the variable *percent up slope*, strongly influenced the locations of burrowing owl burrows, golden eagle flight locations, and red-tailed hawk and American kestrel hovering and kiting locations (Figures 13 and 14). Whereas golden eagle flights did not relate with *percent up slope* over valley bottoms and lower slopes, they increased in frequency with increasing percent up slope values from halfway up the slopes, peaking at the tops of slopes (Figure 13). Hovering and kiting by red-tailed hawks and American kestrels was most commonly observed high on slopes, though American kestrel hovering and kiting flights peaked between 90% and <100% of the tops of slopes. Burrowing owl nest burrows were most numerous between about 10% and 25% of the way up slopes (Figure 14).

FL models were composed of three to four predictor variables per species (Tables 4-7). Each FL model yielded value ranges from 0 to 1 per predictive variable, which we then weighted and summed as follows:

	Maximum Score Possible
Golden eagle score = 2U + A + 3HP	6
Red-tailed hawk score = 2U + 4A + 2HS + 2HP	10
American kestrel score = 3U + 2A + 3HS	8
Burrowing owl score = 3U + 2EV + ED	6

where U represented *percent up slope*, A represented *aspect*, HP represented grid cells within hazard polygons, HS represented *hill size*, EV represented elevation of nearest *valley polygon*,

and ED = *elevation difference*, or the difference in elevation between the nearest ridge crest and nearest valley bottom. Weights were based on the ratio of observed to expected numbers of bird observations among grid cells with FL membership values of 1. Summed, weighted scores were classified using natural breaks to arrive at 4 FL surface classes per species (Tables 8-11, Figure 15).

Table 4. Golden eagle fuzzy logic membership functions of grid cells belonging to the set of cells with golden eagle observations from 15 stations in Vasco Caves Regional Preserve, where observations were weighted by detection functions derived from distances of grid cells from the observer, visible volume of airspace within the maximum survey radius from each station, number of observation sessions per station, and degree of overlap of observable grid cells from multiple stations.

Value of variable Y for *i*th grid cell	**Basis of membership function**	**Membership function of grid cell belonging to set with bird observations**
Y = Percent up slope		
$86.70 < Y \leq 100$	Within $\bar{x}$ & 1 SD > $\bar{x}$	1
$60.20 < Y < 86.70$	Within 2 SD of $\bar{x}$	$0.5 \times (1 - COS(\pi \times (Y - 60.20) / (86.70 - 60.20)))$
		Undefined
$Y < 60.20$	>2 SD from $\bar{x}$	0
Y = Aspect		
$72.94 < Y < 89.77$ & $268.44 < Y < 285.35$	>1 SD from $\bar{x}$ in both 180˚ hemispheres	1
$32.29 < Y_1 < 72.94$; $230.01 < Y_2 < 268.44$	Within 1 SD & 1 SE < $\bar{x}$ in both 180˚ hemispheres	$0.5 \times (1 - COS(\pi \times (Y - 32.29) / (72.94 - 32.29)))$; $0.5 \times (1 - COS(\pi \times (Y - 230.01) / (268.435 - 230.01)))$
$89.77 < Y_1 < 130.43$; $285.35 < Y_2 < 323.78$	Within 1 SD & 1 SE > $\bar{x}$ in both 180˚ hemispheres	$0.5 \times (1 + COS(\pi \times (Y - 89.77) / (130.43 - 89.77)))$; $0.5 \times (1 + COS(\pi \times (Y - 285.35) / (323.78 - 285.35)))$
$Y < 32.29$ or $Y > 130.43$ $Y < 230.01$ or $Y > 323.78$	Within 2 SE of $\bar{x}$ in both 180-degree hemispheres	0
Y = Hazard polygon		
Y = Within polygon	Not applicable	1

Table 5. Red-tailed hawk fuzzy logic membership functions of grid cells belonging to the set of cells with red-tailed hawk observations from 15 stations in Vasco Caves Regional Preserve, where observations were weighted by detection functions derived from distances of grid cells from the observer, visible volume of airspace within the maximum survey radius from each station, number of observation sessions per station, and degree of overlap of observable grid cells from multiple stations.

Value of variable Y for *i*th grid cell	**Basis of membership function**	**Membership function of grid cell belonging to set with bird observations**
Y = Percent up slope		
73.18 < Y < 102.79	Within 5 SE < $\bar{x}$ & 1 SD > $\bar{x}$	1
43.89 < Y < 73.18	Within 5 SE & 1.5 SD < $\bar{x}$	0.5 × (1 - COS(π × (Y - 43.89) / (73.18 - 43.89)))
102.79 < Y < 114.57	Within 1 SD & 1.5 SD > $\bar{x}$	0.5 × (1 + COS(π × (Y - 102.79) / (114.57 - 102.79)))
Y < 43.89	>1.5 SD from $\bar{x}$	0
Y = Aspect (>100˚)		
209.27 < Y < 280.72	Within 10 SE of $\bar{x}$	1
128.80 < Y < 209.27	Within 1.5 SD & 8 SE < $\bar{x}$	0.5 × (1 - COS(π × (Y - 128.80) / (209.27 - 128.80)))
280.72 < Y < 361.20	Within 8 SE & 1.5 SD > $\bar{x}$	0.5 × (1 + COS(π × (Y - 280.72) / (361.20 - 280.72)))
Y < 128.80 or Y > 361.20	>2 SD from $\bar{x}$	0
Y = Hill size		
59.52 < Y < 86.17	Within $\bar{x}$ & 1 SD > $\bar{x}$	1
19.55 < Y < 59.52	Within $\bar{x}$ & 1.5 SD < $\bar{x}$	0.5 × (1 - COS(π × (Y - 19.55) / (59.52 - 19.55)))
86.17 < Y < 99.49	Within 1 & 1.5 SD > $\bar{x}$	0.5 × (1 + COS(π × (Y - 86.17) / (99.49 - 86.17)))
Y < 19.55 or Y > 99.49	>1.5 SD from $\bar{x}$	0
Y = Hazard polygon		
Y = Within polygon	Not applicable	1

Table 6. American kestrel fuzzy logic membership functions of grid cells belonging to the set of cells with American kestrel observations from 15 stations in Vasco Caves Regional Preserve, where observations were weighted by detection functions derived from distances of grid cells from the observer, visible volume of airspace within the maximum survey radius from each station, number of observation sessions per station, and degree of overlap of observable grid cells from multiple stations.

Value of variable Y for *i*th grid cell	**Basis of membership function**	**Membership function of grid cell belonging to set with bird observations**
Y = Percent up slope		
80.86 < Y < 99.04	Within $\bar{x}$ & 10 SE > $\bar{x}$	1
56.13 < Y < 80.86	Within $\bar{x}$ & 1 SD < $\bar{x}$	0.5 × (1 - COS(π × (Y - 56.13) / (80.86 - 56.13)))
99.04 < Y < 100	Within 10 SE > $\bar{x}$ & 100	0.5 × (1 + COS(π × (Y - 99.04) / (100 - 99.04)))
Y < 56.13	>1 SD from $\bar{x}$	0
Y = Aspect		
165.67 < Y < 264.64	Within 8 SE of $\bar{x}$	1
88.96 < Y < 165.67	Within 1.5 SD & 8 SE < $\bar{x}$	0.5 × (1 - COS(π × (Y - 88.96) / (165.67 - 88.96)))
264.64 < Y < 341.35	8 SE to 1.5 SD > $\bar{x}$	0.5 × (1 + COS(π × (Y - 264.64) / (341.35 - 264.64)))
Y < 88.96 or Y > 341.35	>1.5 SD from $\bar{x}$	0
Y = Hill size		
60.30 < Y < 83.16	Within 7 SE of $\bar{x}$	1
38.42 < Y < 60.30	Within 1.5 SD & 7 SE < $\bar{x}$	0.5 × (1 - COS(π × (Y - 38.42) / (60.30 - 38.42)))
83.16 < Y < 105.04	Within 7 SE & 1.5 SD > $\bar{x}$	0.5 × (1 + COS(π × (Y - 83.16) / (105.04 - 83.16)))
Y < 38.42 or Y > 105.04	>1.5 SD from $\bar{x}$	0

Table 7. Burrowing owl fuzzy logic membership functions of grid cells belonging to the set of cells with burrowing owl nest burrows mapped within Vasco Caves Regional Preserve.

Value of variable Y for *i*th grid cell	**Basis of membership function**	**Membership function of grid cell belonging to set with bird observations**
Y = Percent up slope		
5.92 < Y < 31.82	Within - 5 SD & $\bar{x}$	1
2.10 < Y < 5.92	Within 1 SD + 1 SE & 1 SD < $\bar{x}$	0.5 × (1 - COS(π × (Y - 2.10) / (5.92 - 2.10)))
31.82 < Y < 61.53	Within $\bar{x}$ & 1 SD + 1 SE > $\bar{x}$	0.5 × (1 + COS(π × (Y - 31.82) / (61.53 - 31.82)))
Y < 2.10 or Y > 61.523	>1 SD + 1 SE away from $\bar{x}$	0
Y = Elevation of nearest valley bottom polygon		
0 ≤ Y < 135.19	>2 SD > $\bar{x}$	1
		Undefined
135.19 < Y < 175.77	Within 2 SD & 2 SE > $\bar{x}$	0.5 × (1 + COS(π × (Y - 135.19) / (175.77 - 135.19)))
Y > 175.77	Within 2 SE > $\bar{x}$	0
Y = Elevation difference		
16.79 < Y < 32.89	Within 4 SE of $\bar{x}$	1
13.93 < Y < 16.79	Within 1 SD & 4 SE < $\bar{x}$	0.5 × (1 - COS(π × (Y - 13.93) / (16.79 - 13.93)))
32.89 < Y < 35.75	Within 4 SE & 1 SD > $\bar{x}$	0.5 × (1 + COS(π × (Y - 32.89) / (35.75 - 32.89)))
Y < 13.93 or Y > 35.75	>1 SD from $\bar{x}$	0

Table 8. Fuzzy logic model of golden eagle flight locations, model performance within the masked study area, and percentage of the project area included in each FL likelihood surface class.

FL likelihood surface class	FL model value range	Sum weighted observations	Masked study area (%)	Observed ÷ expected no. of observations	Project area (%)
1	0-1	343	54.7	0.59	57.4
2	>1-2.1	404	29.2	1.30	29.2
3	>2.1-3	206	10.7	1.80	9.9
4	>3	95	3.7	2.39	3.5

Table 9. Fuzzy logic model of red-tailed hawk hovering and kiting locations, model performance within the masked study area, and percentage of the project area included in each FL likelihood surface class.

FL likelihood surface class	FL model value range	Sum weighted observations	Masked study area (%)	Observed ÷ expected no. of observations	Project area (%)
1	0-4	246	69.3	0.39	70.4
2	>4-6	228	21.2	1.19	20.2
3	>6-7.799	239	8.0	3.31	8.2
4	7.8-10	189	1.6	13.10	1.3

Table 10. Fuzzy logic model of American kestrel hovering and kiting locations, model performance within the masked study area, and percentage of the project area included in each FL likelihood surface class.

FL likelihood surface class	FL model value range	Sum weighted observations	Masked study area (%)	Observed ÷ expected no. of observations	Project area (%)
1	0-4.399	265	77.8	0.36	83.5
2	4.4-5.499	233	12.4	1.97	10.3
3	5.5-7.499	228	7.9	3.02	5.1
4	7.5-8	230	2.0	12.03	1.2

Table 11. Fuzzy logic model of burrowing owl nest burrow locations, model performance within the 543-ha Vasco Caves and Souza parcels that were searched by Albion Environmental in 2006-2007, and percentage of the project area included in each FL likelihood surface class.

FL likelihood surface class	FL model value range	Sum observations	Masked study area (%)	Observed ÷ expected no. of observations	Project area (%)
1	0-3.999	14	79.5	0.38	74.9
2	4-4.999	5	10.8	1.01	8.7
3	5-5.999	13	6.1	4.63	10.5
4	6	14	3.7	8.23	5.8

Predicted Hazard Zones in the Tres Vaqueros Project Area

The predictive models developed in the masked study area were projected to the Tres Vaqueros project area, part of which included the masked study area and part of which was immediately adjacent to the study area to the west and northwest (Figures 16-19). A map of hazard polygons was developed separately from the predictive models based directly on bird utilization data (Figure 20), and these polygons were incorporated into the FL models for golden eagle and red-tailed hawk.

Comparing percentages between the masked study area and the project area, the distribution of FL likelihood surface classes appeared similar for flying golden eagles and hovering/kiting red-tailed hawks (Tables 8 and 9), but the project area might not have as many hovering/kiting American kestrels as the study area did (Table 10). The distribution of burrowing owl nest burrows may be similar in overall numbers (Table 11), but most of the project area burrows likely will occur in the lower elevation landscape in the northeastern and eastern aspects of the project area.

DISCUSSION

We produced simple models of golden eagle flights, red-tailed hawk and American kestrel hovering and kiting, and of burrowing owl nest burrow locations. These models can be used to guide wind turbine siting intended to minimize encounter frequencies between raptors and operating wind turbines, although significant uncertainties in the mechanisms of collisions could reduce the effectiveness of the models. For example, we suspect but we do not know that where golden eagles most often fly corresponds with where they get killed by wind turbines, nor do we know that where red-tailed hawks and American kestrels hover most often is also where they get killed (Smallwood et al. 2009b). We suspect but we do not know that the locations of burrowing owl nest burrows correspond with wind turbine-caused fatalities (Smallwood and Neher 2009, Smallwood et al. 2007, 2009a,c). It may be that rarely performed behaviors cause the majority of wind turbine collisions, and we may not have characterized those rare behaviors. However, until these uncertainties are eliminated, a reasonable first assumption is that our model predictions should correspond with increased hazard of wind turbine collisions should wind turbines be installed where our models predict highest activity levels.

We recommend not locating wind turbines in the hazard polygons we overlayed on ridge saddles, notches, and benches, or where there are other breaks in the slope of the ridge or hill. We also recommend avoiding the lowest terrain, such as in valley or ravine bottoms. We recommend avoiding areas mapped as FL surface class 4 for any of the target species, and that caution be exercised within areas mapped as FL surface class 3. Increasing the distances between wind turbines and FL surface classes 3 and 4 will likely decrease future fatalities of raptors.

ACKOWLEDGEMENTS

We thank East Bay Regional Park District and the California Energy Commission's Public Interest Energy Research program for funding. We thank Jack Barclay, Lindsay Harmon, Brian Karas, and Heather Snively for data collection. We also thank Linda Maples, Sherrity McBane, Leah Neher, and Gina Neher for GIS data entry.

REFERENCES

Anderson, R., M., Morrison, K. Sinclair, D. Strickland. 1999. Studying wind energy and bird interactions: A guidance document. National Wind Coordinating Committee. Washington, D.C. 87 pp.

California Energy Commission and California Department of Fish and Game (CEC & CDFG). 2007. California Guidelines for Reducing Impacts to Birds and Bats from Wind Energy Development. Draft Staff Report CEC-700-2007-008-SD, Sacramento, California.

Gauthreaux, S. A. 1996. Suggested practices for monitoring bird populations, movements and mortality in wind resource areas. In: Proceedings of National Avian-Wind Power Planning Meeting II. Palm Springs, California, 20-22 Sept. 1995. Prepared for the Avian Subcommittee of the National Wind Coordination Committee by RESOLVE Inc., Washington, DC, and LGL Ltd., King City, Ont. 152 pp.

Insignia Environmental. 2009. 2008/2009 Annual Report for the Buena Vista Avian and Bat Fatality Monitoring Project. Unpublished report prepared for County of Contra Costa, Martinez, California.

Kainz, W. 2004. Fuzzy logic and applications in GIS. 2004 ESRI International User Conference. Department of Geography and Regional Research, University of Vienna, Austria.

Smallwood, K. S. and B. Karas. 2009. Avian and Bat Fatality Rates at Old-Generation and Repowered Wind Turbines in California. Journal of Wildlife Management 73:1062-1071.

Smallwood, K. S. and L. Neher. 2004. Repowering the APWRA: Forecasting and minimizing avian mortality without significant loss of power generation. California Energy Commission,

Public Interest Energy Research – Environmental Area Report CEC-500-2005-005, Sacramento, California, USA.

Smallwood, K. S., and L. Neher. 2009. Map-Based Repowering of the Altamont Pass Wind Resource Area Based on Burrowing Owl Burrows, Raptor Flights, and Collisions with Wind Turbines. Final Report to the California Energy Commission, Public Interest Energy Research – Environmental Area, Contract No. CEC-500-2009-065. Sacramento, California. 63 pp. http://www.energy.ca.gov/2009publications/CEC-500-2009-065/CEC-500-2009-065.PDF

Smallwood, K. S., C. G. Thelander. 2008. Bird Mortality in the Altamont Pass Wind Resource Area, California. Journal of Wildlife Management 72:215-223.

Smallwood, K. S., L. Neher, and D. A. Bell. 2009a. Map-based repowering and reorganization of a wind resource area to minimize burrowing owl and other bird fatalities. Energies 2009(2):915-943. http://www.mdpi.com/1996-1073/2/4/915

Smallwood, K. S., L. Rugge, and M. L. Morrison. 2009b. Influence of Behavior on Bird Mortality in Wind Energy Developments: The Altamont Pass Wind Resource Area, California. Journal of Wildlife Management 73:1082-1098.

Smallwood, K. S., L. Neher, D. Bell, J. DiDonato, B. Karas, S. Snyder, and S. Lopez. 2009c. Range Management Practices to Reduce Wind Turbine Impacts on Burrowing Owls and Other Raptors in the Altamont Pass Wind Resource Area, California. Final Report to the California Energy Commission, Public Interest Energy Research – Environmental Area, Contract No. CEC-500-2008-080. Sacramento, California. 183 pp. http://www.energy.ca.gov/2008publications/CEC-500-2008-080/CEC-500-2008-080.PDF

Tanaka, K. 1997. An Introduction to Fuzzy Logic for Practical Applications. Springer-Verlag, New York.

U.S. Fish and Wildlife Service. 2003. Interim guidelines to avoid and minimize wildlife impacts from wind turbines. U.S. Department of the Interior, Washington, D.C. 57 pp.

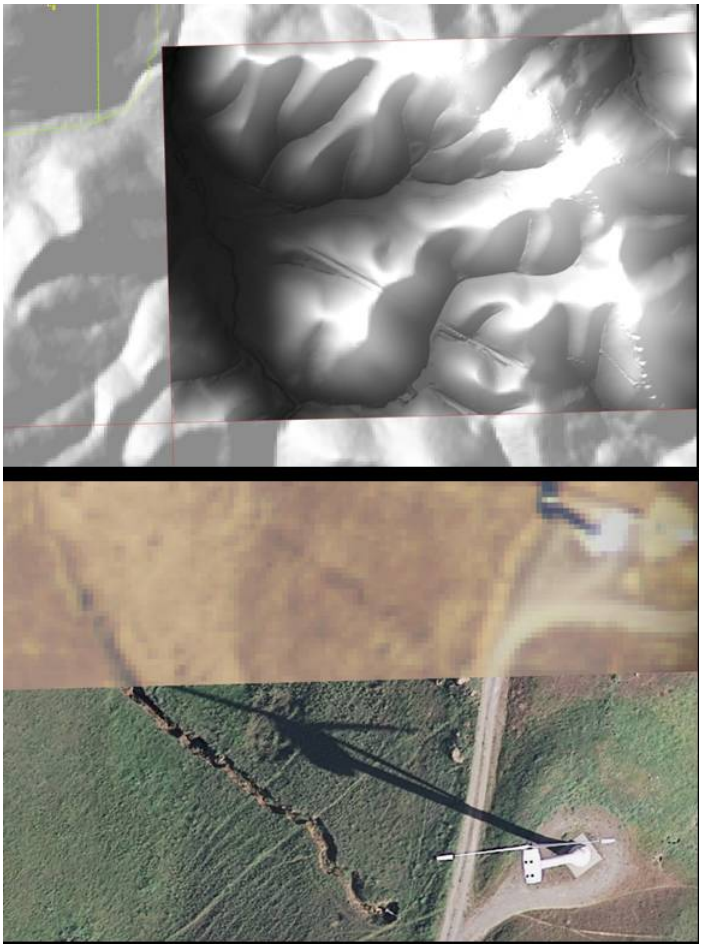

Figure 1. Example differences in imagery of the project area that is now available (hillshade above and photo below), in both cases comparing the 10-m resolution of the imagery that contributed to the Vasco Caves study of 2006-2007 (Smallwood et al. 2009) and the 2-foot imagery that contributed to this study.

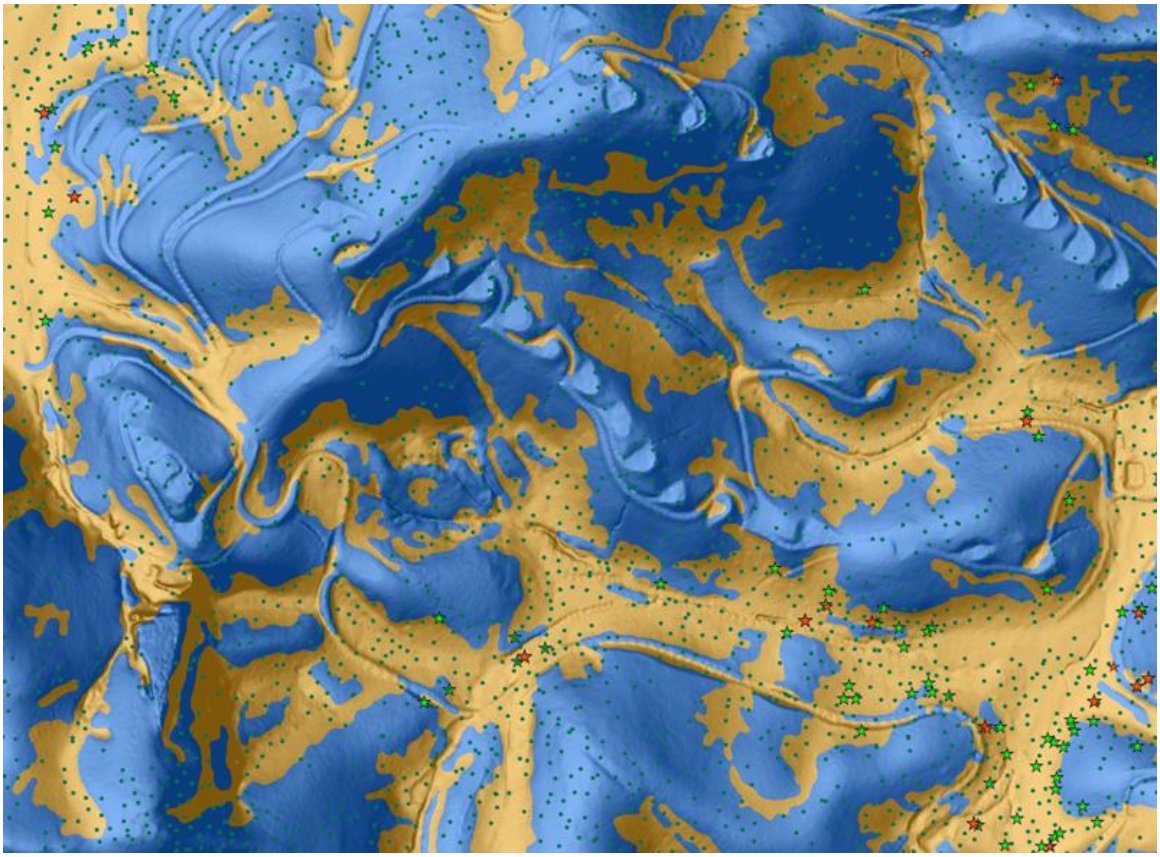

Figure 2. Example representation of differentiation between convex-trending ridge-like features (blue) and concave-trending valley-like features (gold) within the Vasco Caves Regional Preserve and overlain by mammal burrows (greed dots) and burrowing owl nest burrows (stars) mapped in 2006-2007.

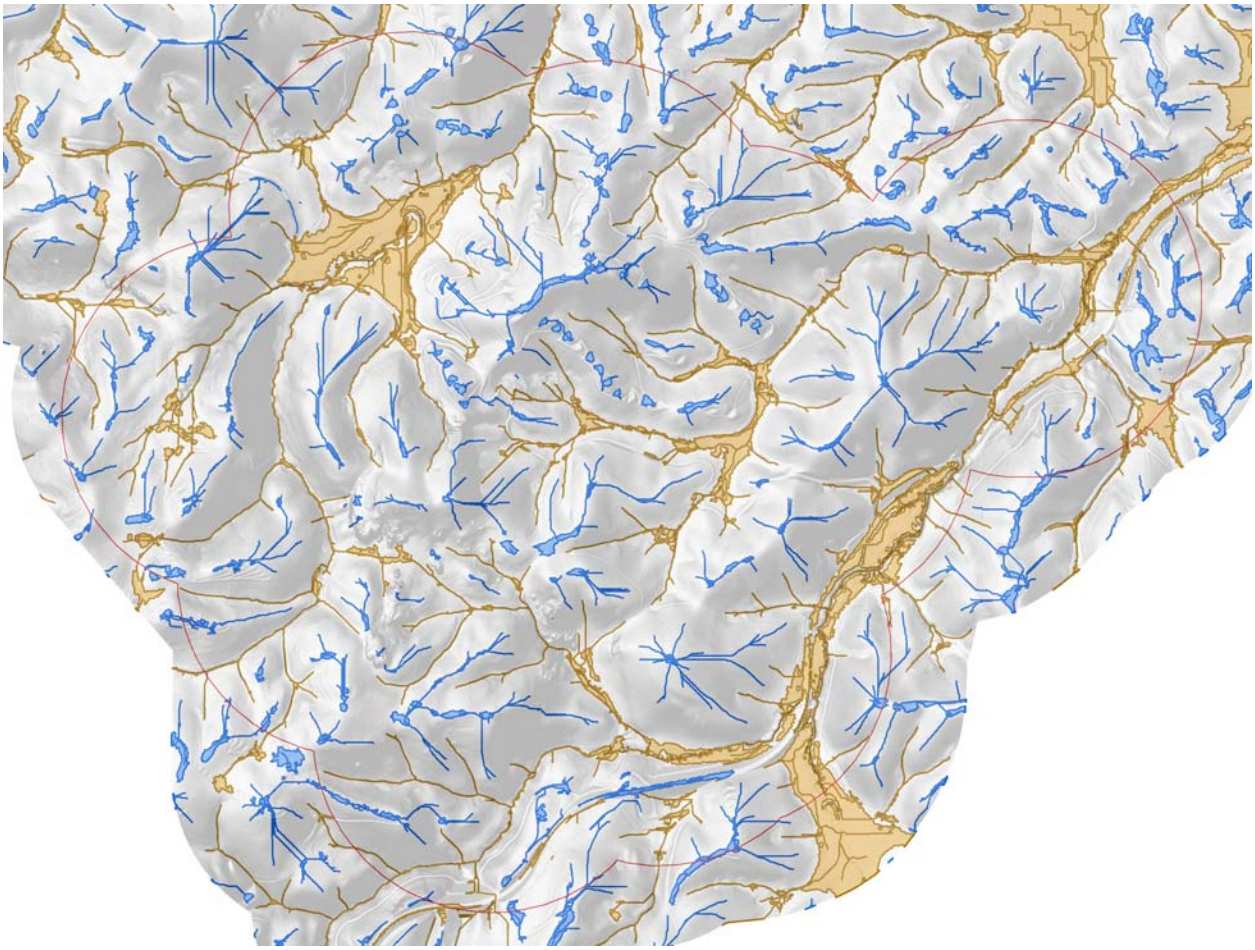

Figure 3. Line features representing ridges and valley bottoms, and significant ridge top and valley bottom polygons, from which revised slope measurements were made.

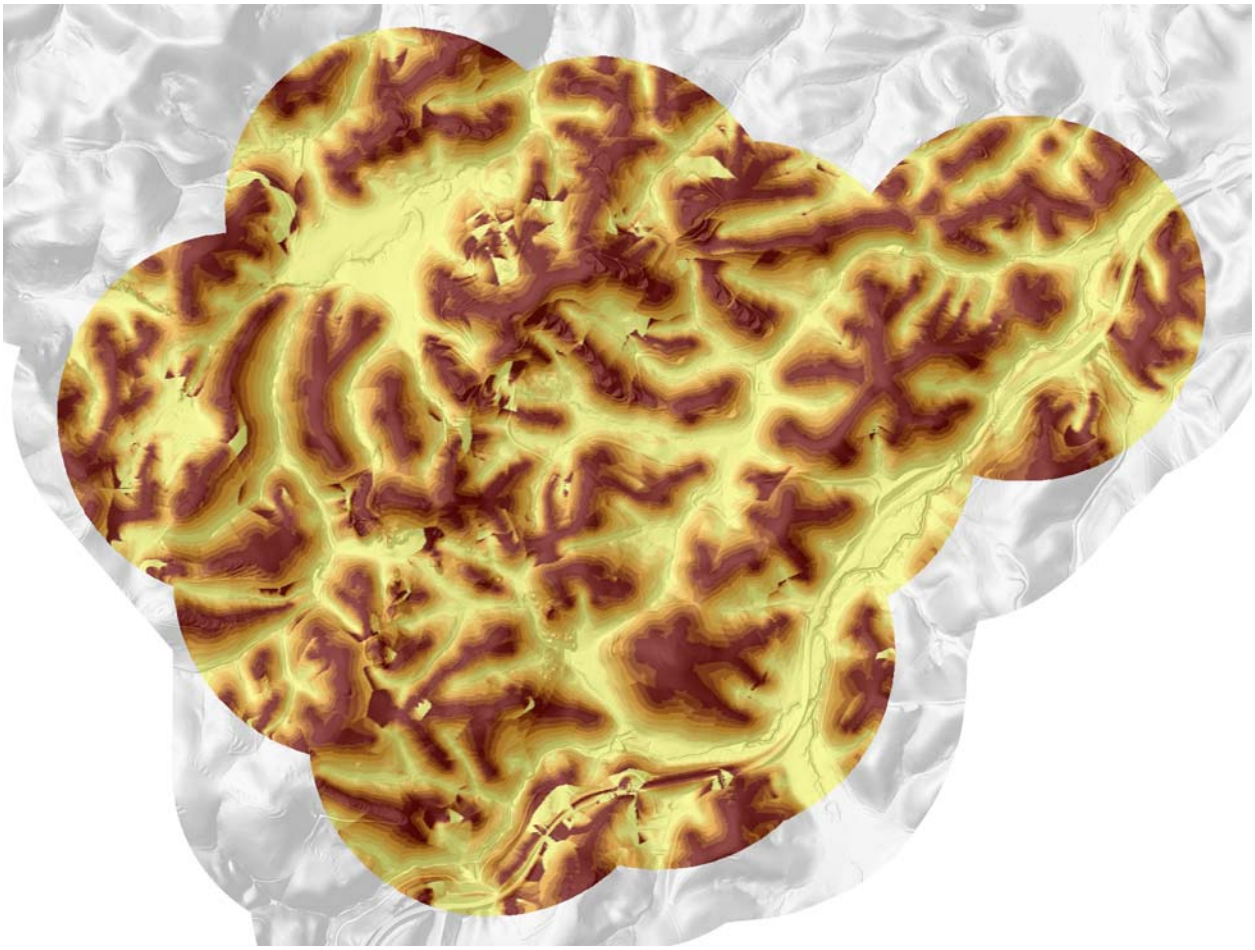

Figure 4. Position on the slope as a percentage of the way from bottom (yellow) to top (maroon) of the slope features in the analytical grid, including all areas surveyed fro birds by Smallwood et al. (2009).

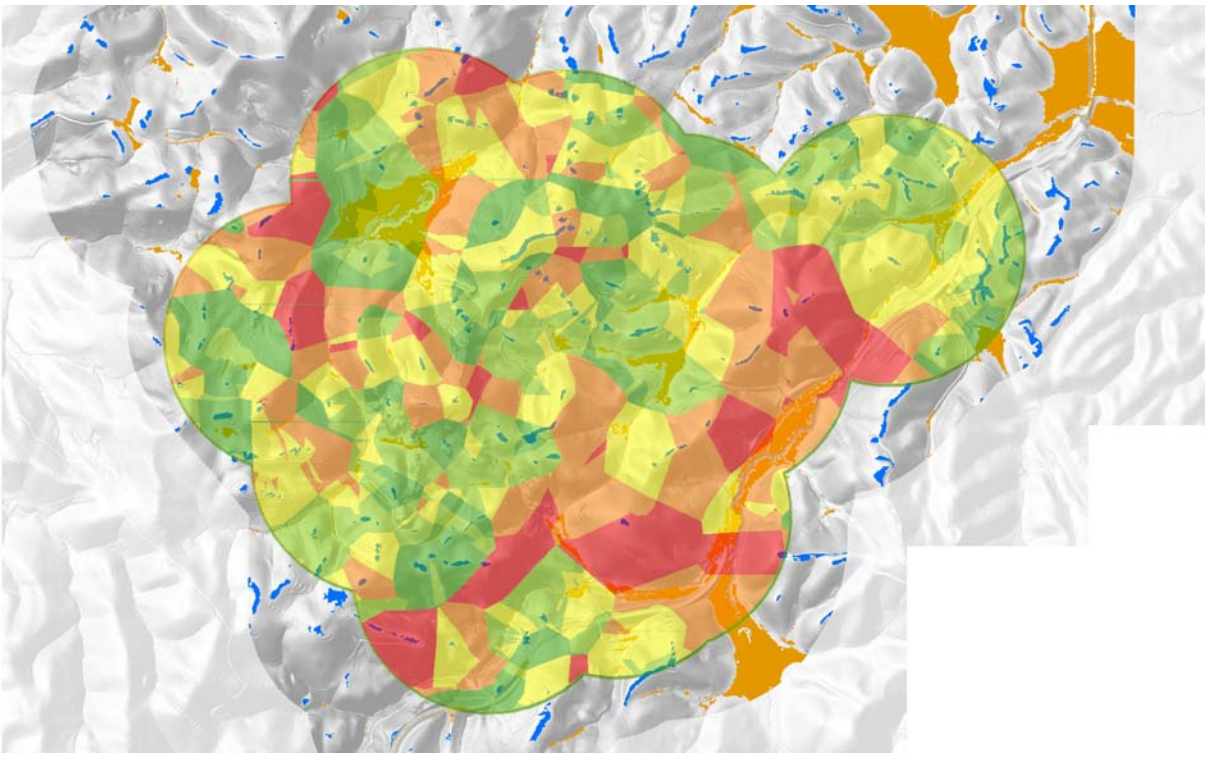

Figure 5. Local topographic influence of the underlying hill slopes, measured as the elevation difference between the nearest valley bottom (gold) and nearest crest of the most prominent hills and ridges in the area (blue), where red denoted largest hills, orange was second to largest, yellow was moderate, light green was second smallest, and dark green was smallest hill features.

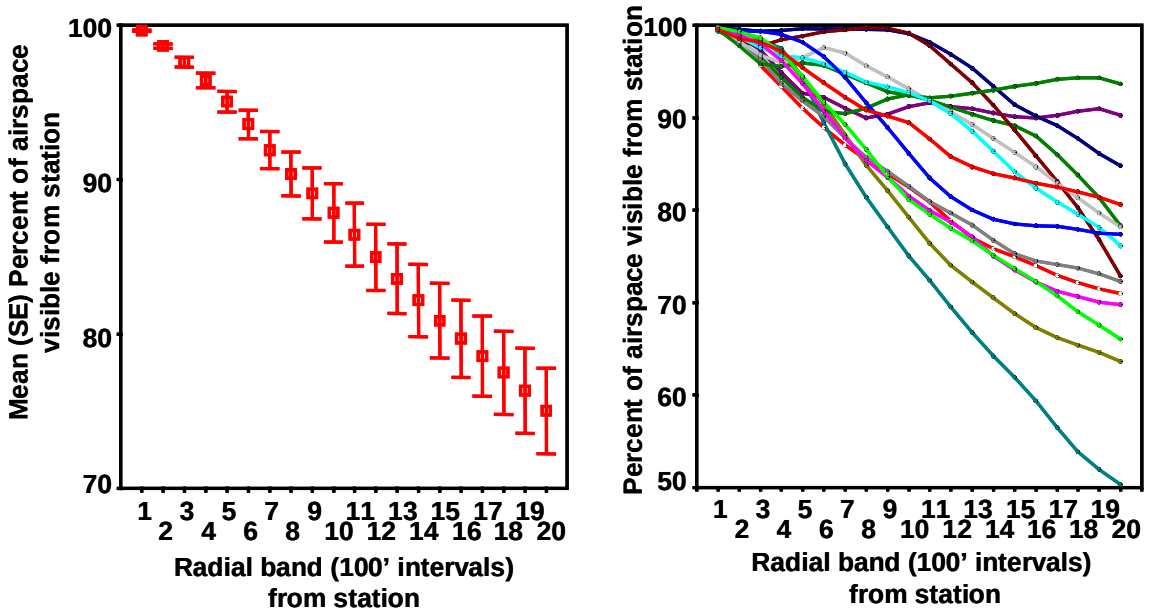

Figure 6. Change in mean (left graph) and station-specific (right graph) percentage of visible volume of airspace within 140-m ceiling and within specific radial bands from the observer (x-axis) among 15 observation stations at Vasco Caves Regional Preserve.

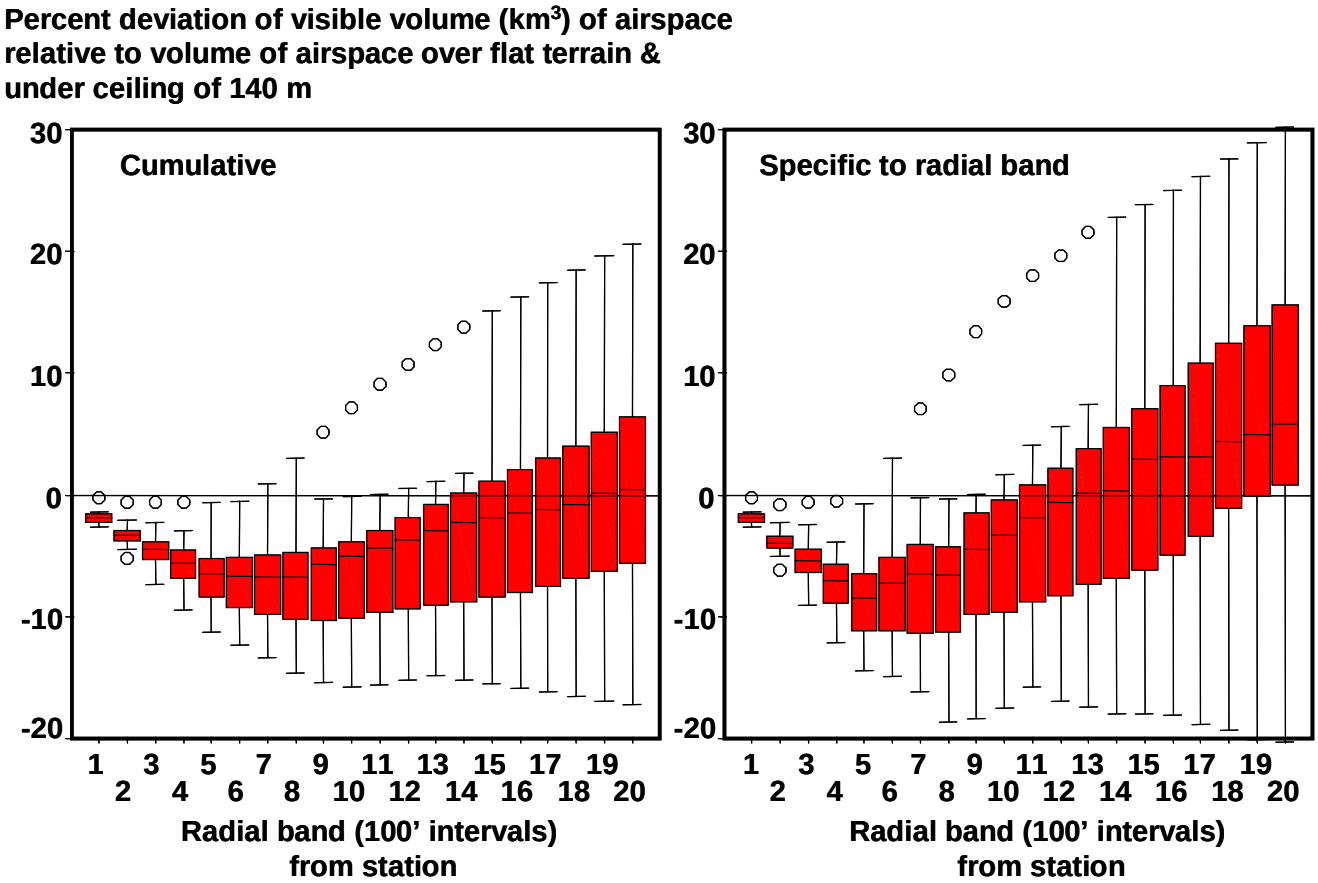

Figure 7. Differences in visible volume of airspace between flat and complex terrain as distance increases from the observer among 15 observation stations in Vasco Caves Regional Preserve, cumulatively (left graph) and specific to radial bands at 100-foot increments from the observer (right graph).

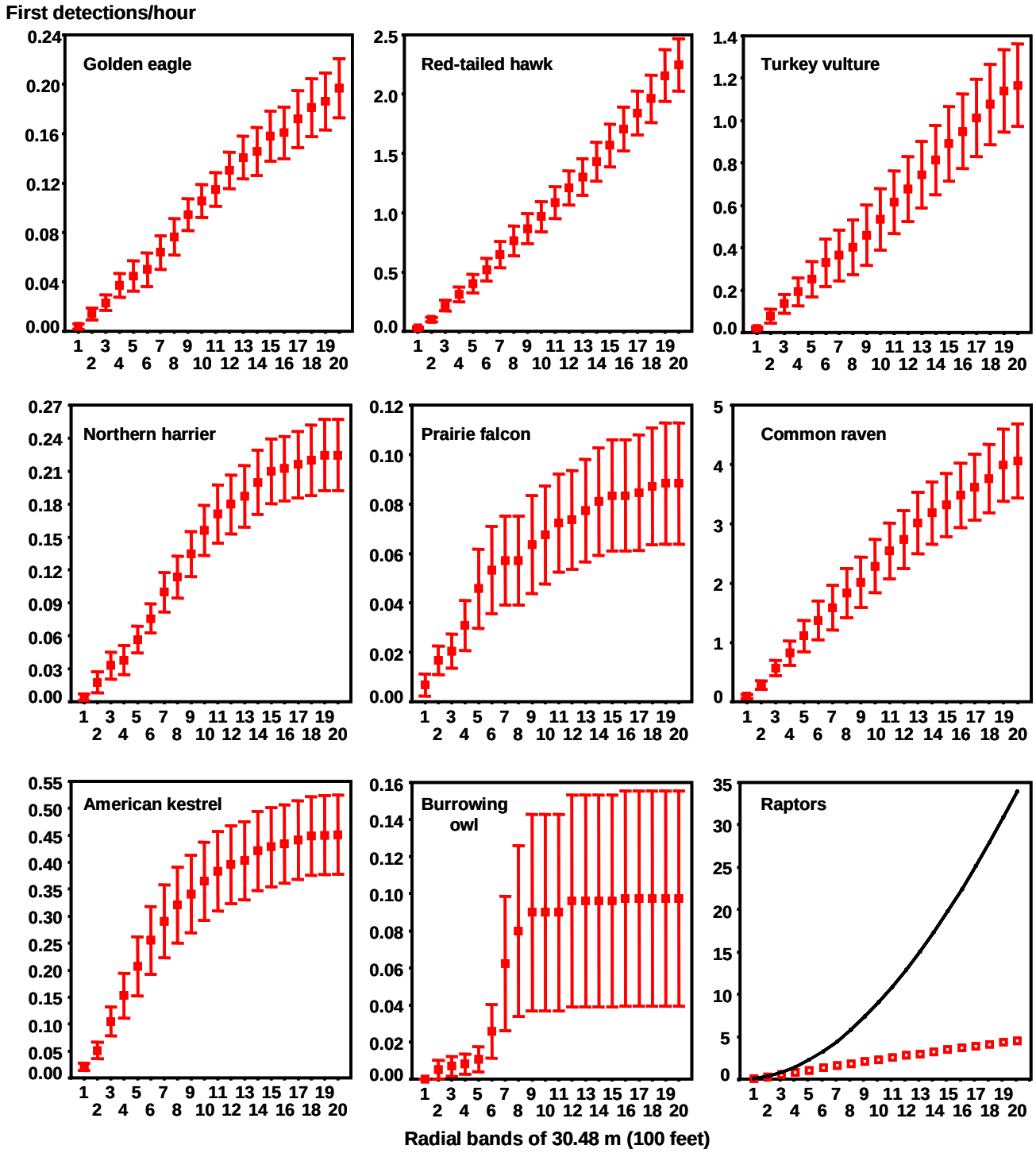

Figure 8. Cumulative mean first detections/hour increased with increasing distance from the observer for golden eagle, red-tailed hawk, turkey vulture, northern harrier, prairie falcon, common raven, American kestrel, burrowing owl, and all raptors as a group in Vasco Caves Regional Preserve, 2006-2007. The solid line in the lower right graph depicts the exponential increase in cumulative detections of raptors, assuming the spatial distribution of raptors was unaffected by the locations of observation stations and detection rate was most accurate within the closest 100 feet.

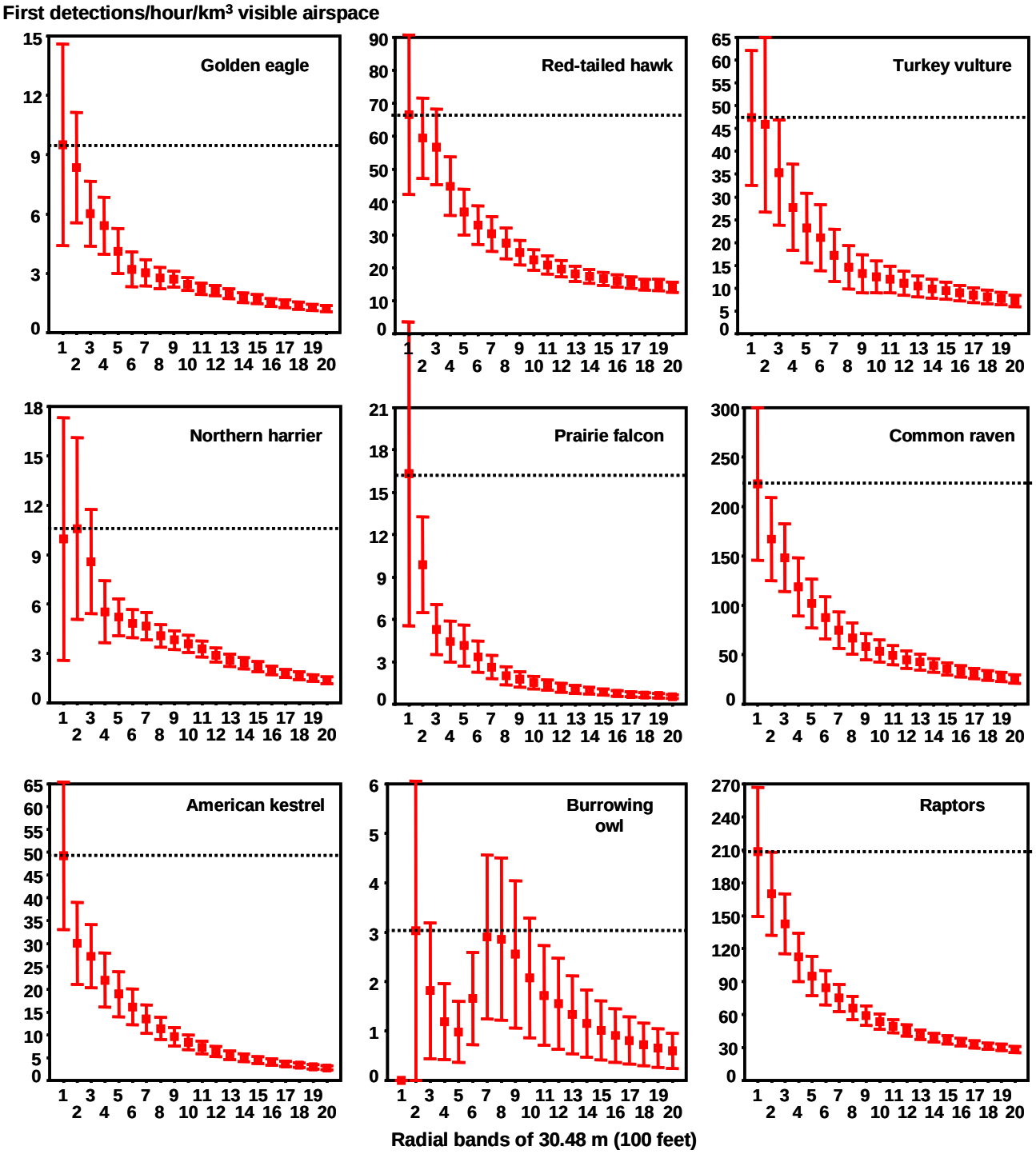

Figure 9. Cumulative mean first detections/hour/km^3 of visible airspace decreased with increasing distance from the observer for golden eagle, red-tailed hawk, turkey vulture, northern harrier, prairie falcon, common raven, American kestrel, burrowing owl, and all raptors as a group in Vasco Caves Regional Preserve, 2006-2007. The horizontal dashed line represented detection rates expected of each species assuming spatial distributions were unaffected by the locations of observation stations and were most accurate within the closest 100 or 200 feet.

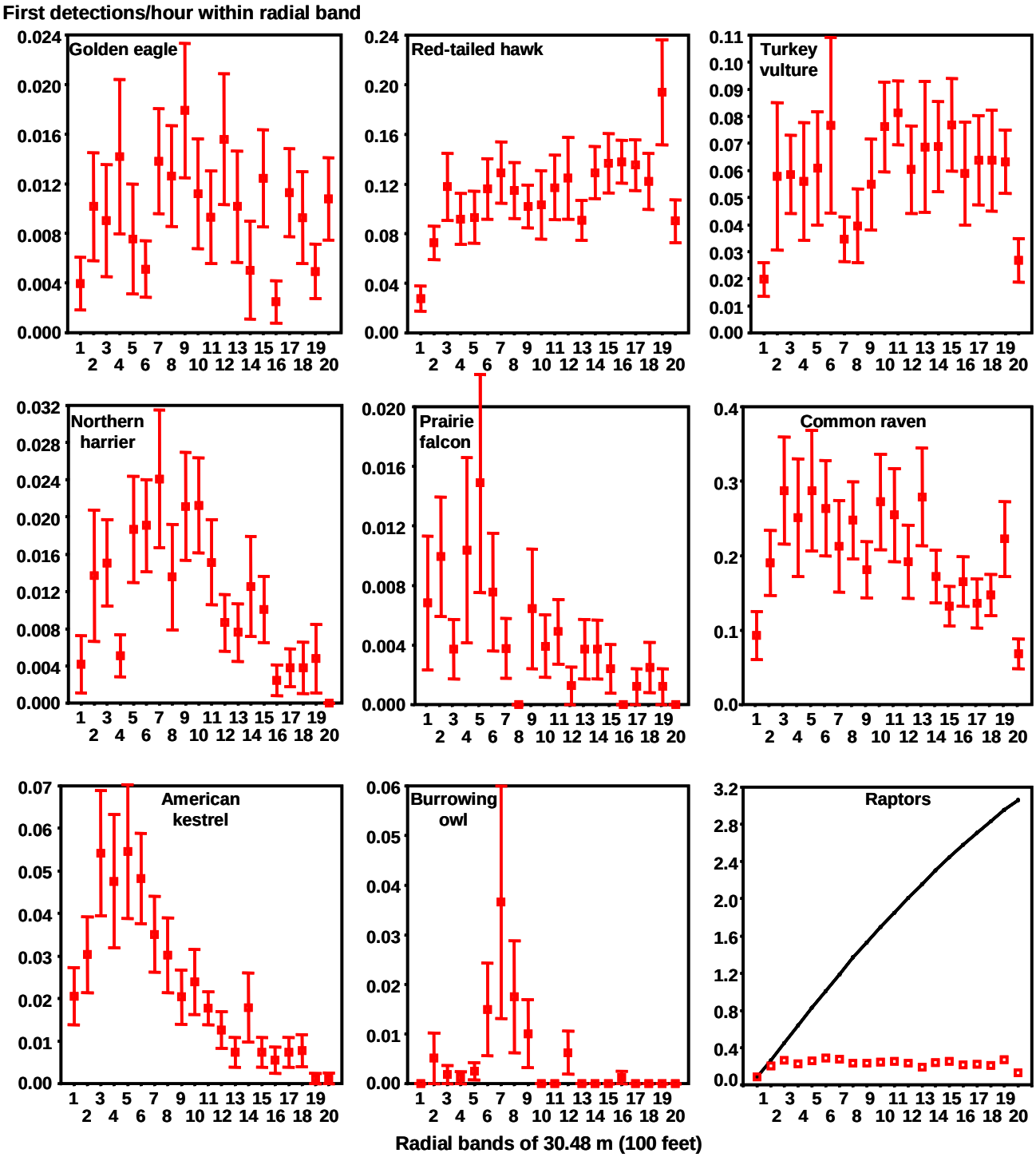

Figure 10. Specific to radial bands, mean first detections/hour changed with increasing distance from the observer for golden eagle, red-tailed hawk, turkey vulture, northern harrier, prairie falcon, common raven, American kestrel, burrowing owl, and all raptors as a group in Vasco Caves Regional Preserve, 2006-2007. The solid line in the lower right graph depicts the increase in detection rates of raptors assuming spatial distributions were unaffected by the locations of observation stations and were most accurate within the closest 100 feet.

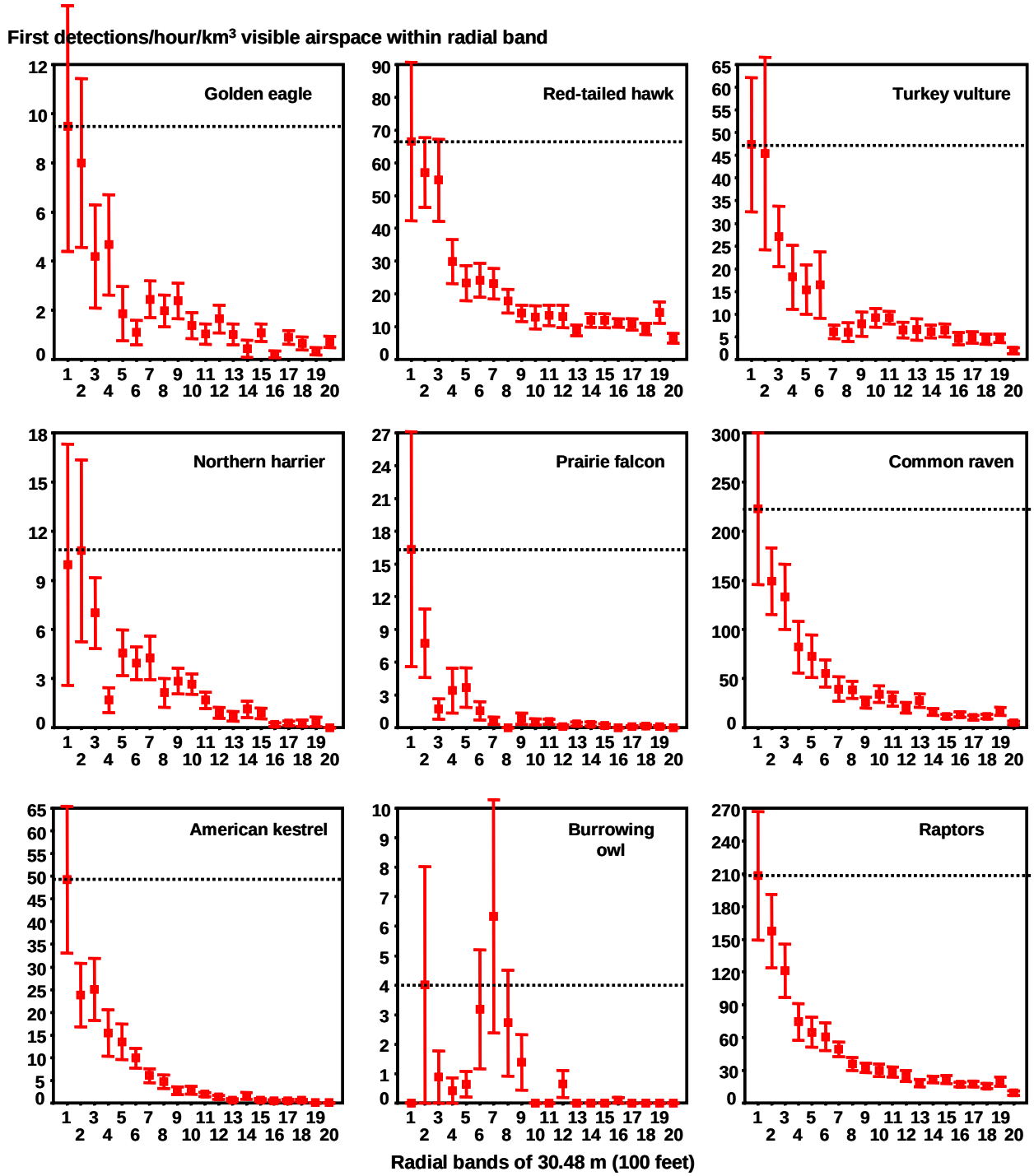

Figure 11. Within specific radial bands, mean first detections/hour/km^3 of visible airspace decreased with increasing distance from the observer for golden eagle, red-tailed hawk, turkey vulture, northern harrier, prairie falcon, common raven, American kestrel, burrowing owl, and all raptors as a group in Vasco Caves Regional Preserve, 2006-2007. The horizontal dashed line represented detection rates expected of each species assuming spatial distributions were unaffected by the locations of observation stations and were most accurate within the closest 100 or 200 feet.

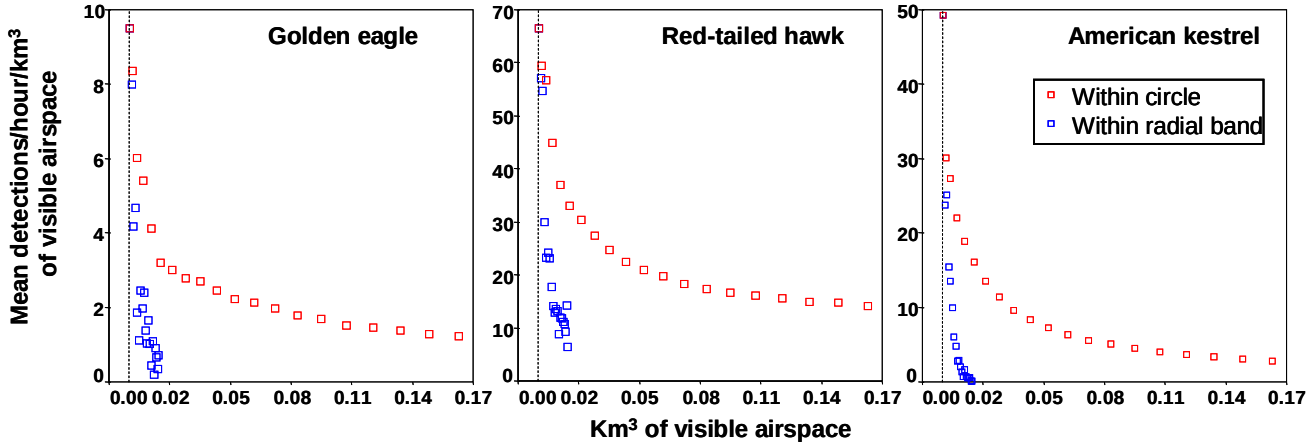

Figure 12. Comparison of declines in detection rates within radial bands (blue) and cumulatively (red) with increasing distance from the observer for three example species – golden eagle, red-tailed hawk, and American kestrel.

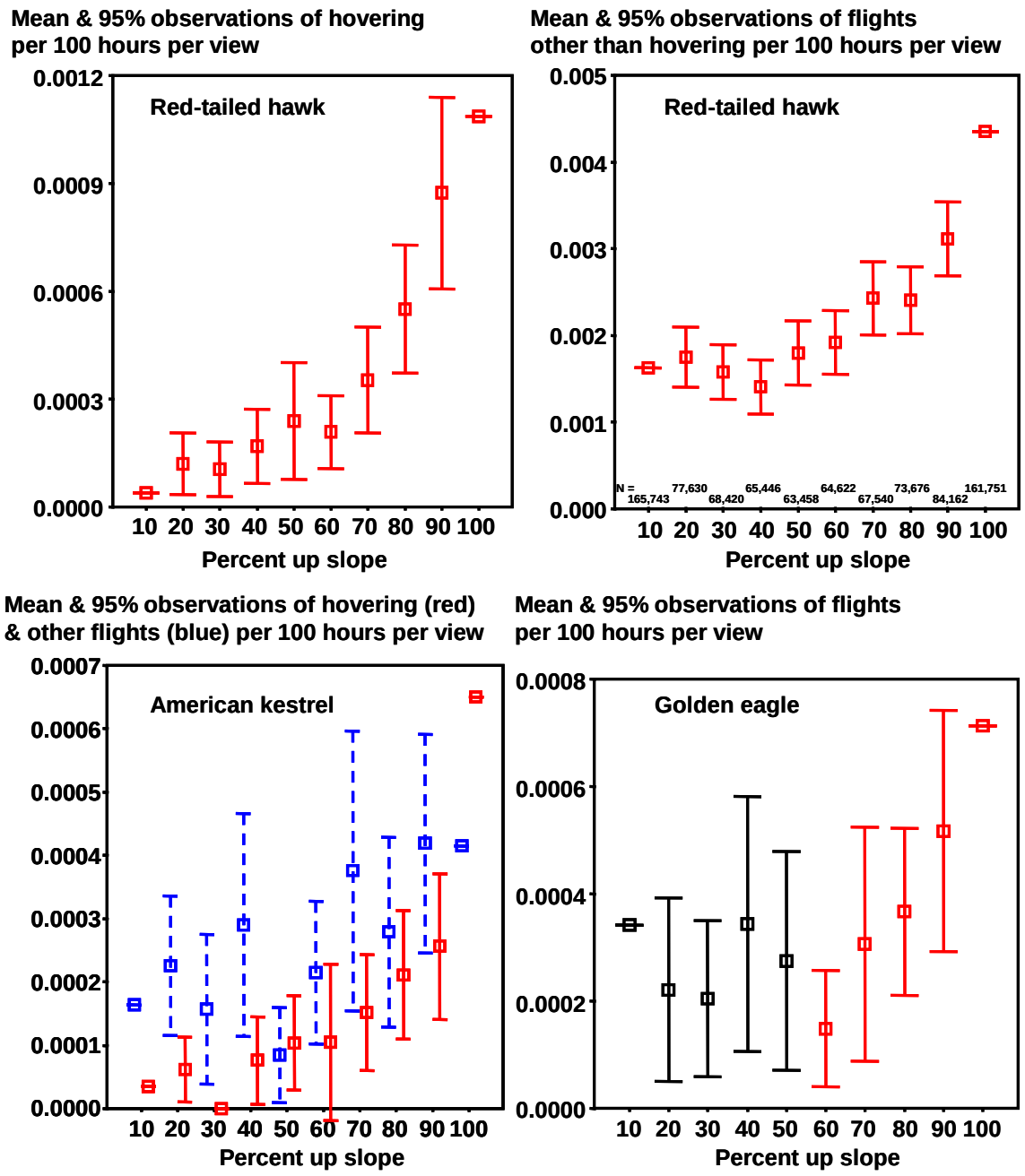

Figure 13. Mean number of red-tailed hawk hovering/kiting flights (top left graph) and all other flights (top right), American kestrel hovering/kiting flights (bottom left, red) and all other flights (bottom left, blue), and golden eagle flights (bottom right) as functions of the grid cell's location as a percentage of the way from the bottom to the top of the slope. Note that mean number of grid cells with golden eagle flights did not grade with slope among grid cells < halfway up the slope (black), whereas it increased with increasingly greater position on the slope among grid cells > halfway up the slope (red).

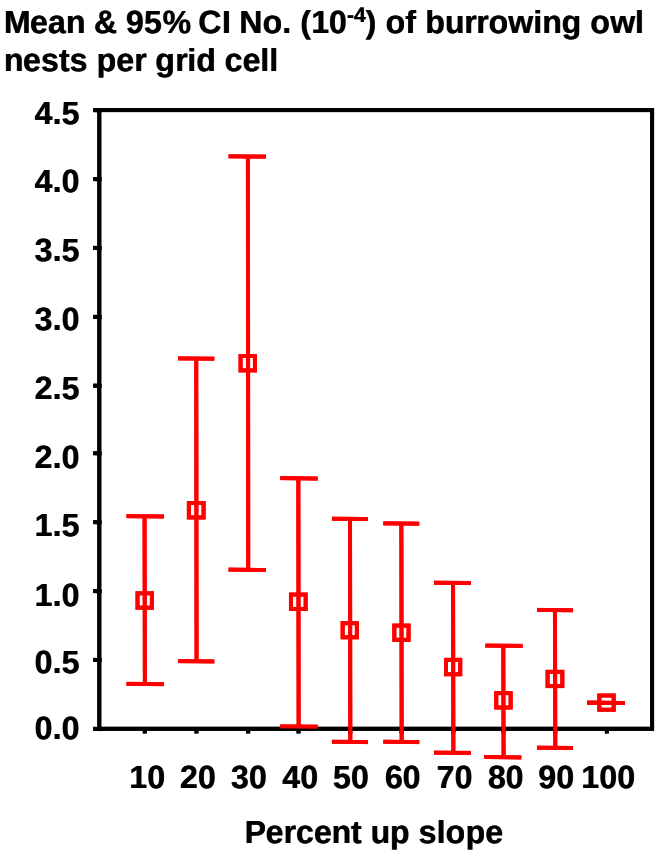

Figure 14. Mean number of grid cells with burrowing owl nest burrows peaked at 20%-30% of the way up the slope.

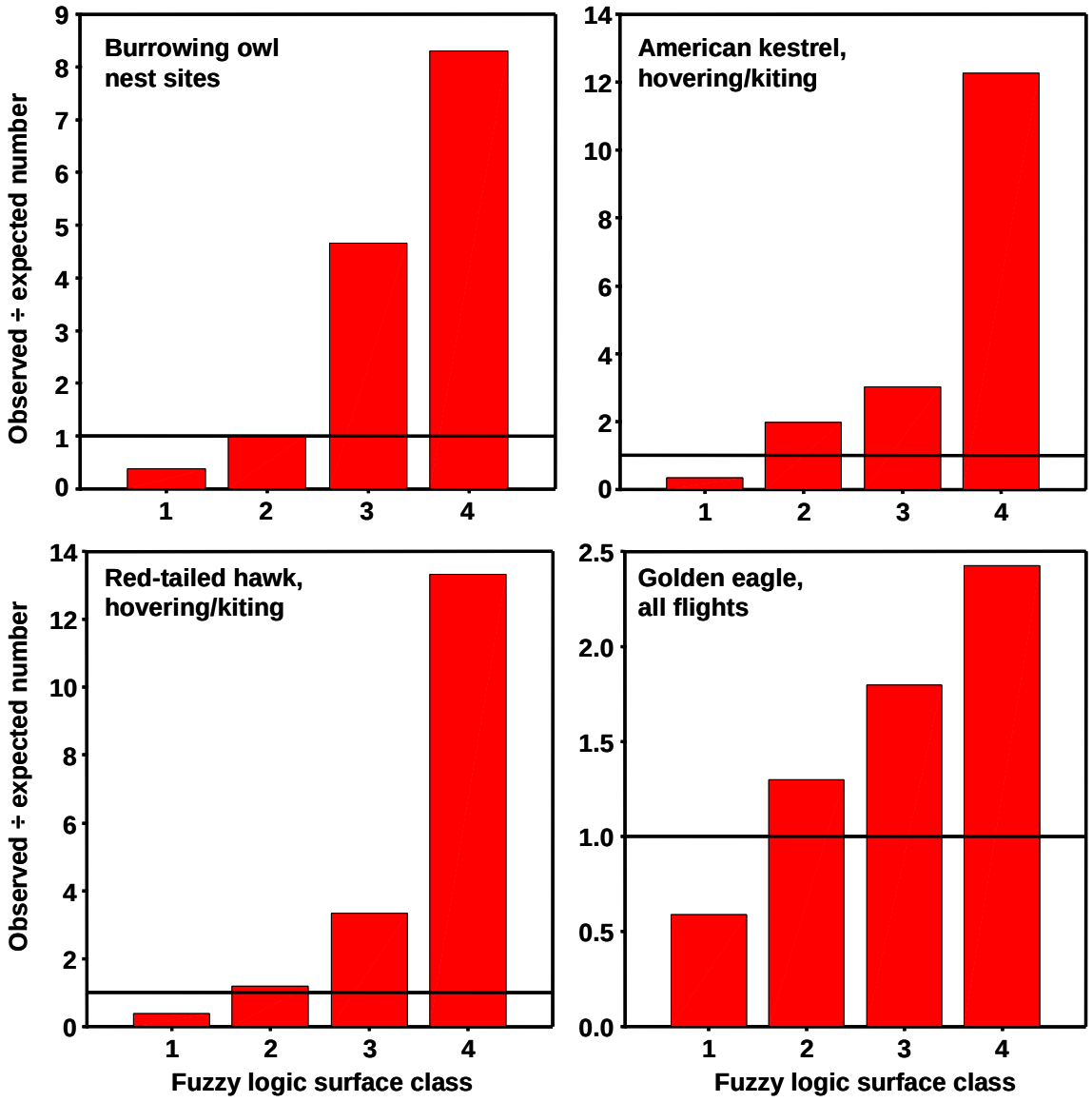

Figure 15. Performance of fuzzy logic models for raptor utilization in Vasco Caves Regional Preserve, including for burrowing owl nest burrow locations (top left graph), American kestrel hovering and kiting flights (top right), red-tailed hawk hovering and kiting flights (bottom left), and all golden eagle flights under the 140-m observation ceiling (bottom right). Horizontal lines at 1.0 represent numbers of observations no greater or lesser other than expected. For example, American kestrel hovering flights in fuzzy logic surface class 4 was 12 times more frequent other than expected.

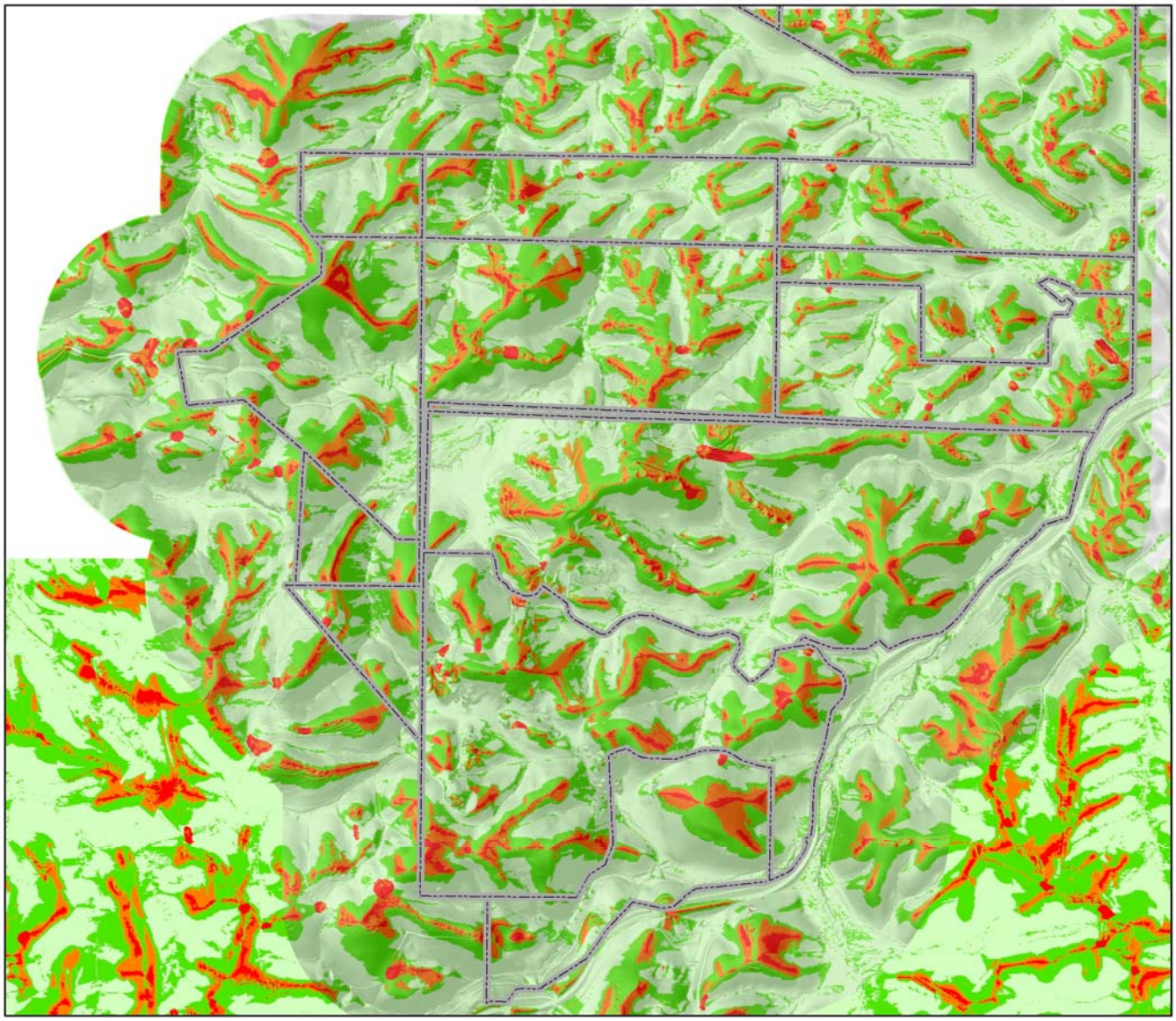

Figure 16. Projection of Fuzzy Logic likelihood surface classes of golden eagle flight locations across entire Tres Vaqueros project area, where red corresponds with the highest likelihood of occurrence, orange corresponds with the second highest likelihood, dark green corresponds with the third highest likelihood, and light green corresponds with the least likelihood.

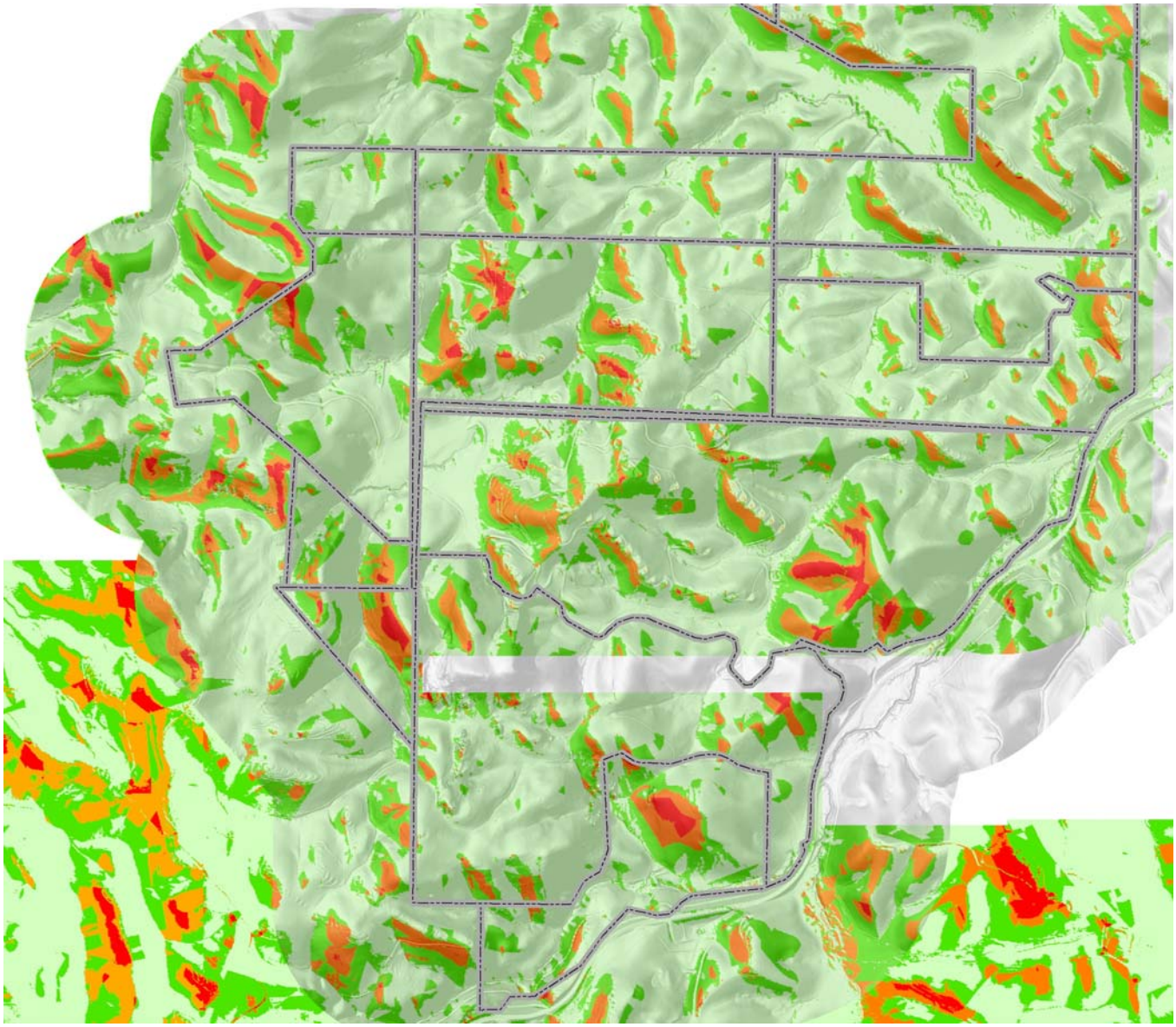

Figure 17. Projection of Fuzzy Logic likelihood surface classes of red-tailed hawk hovering and kiting locations across entire Tres Vaqueros project area, where red corresponds with the highest likelihood of occurrence, orange corresponds with the second highest likelihood, dark green corresponds with the third highest likelihood, and light green corresponds with the least likelihood.

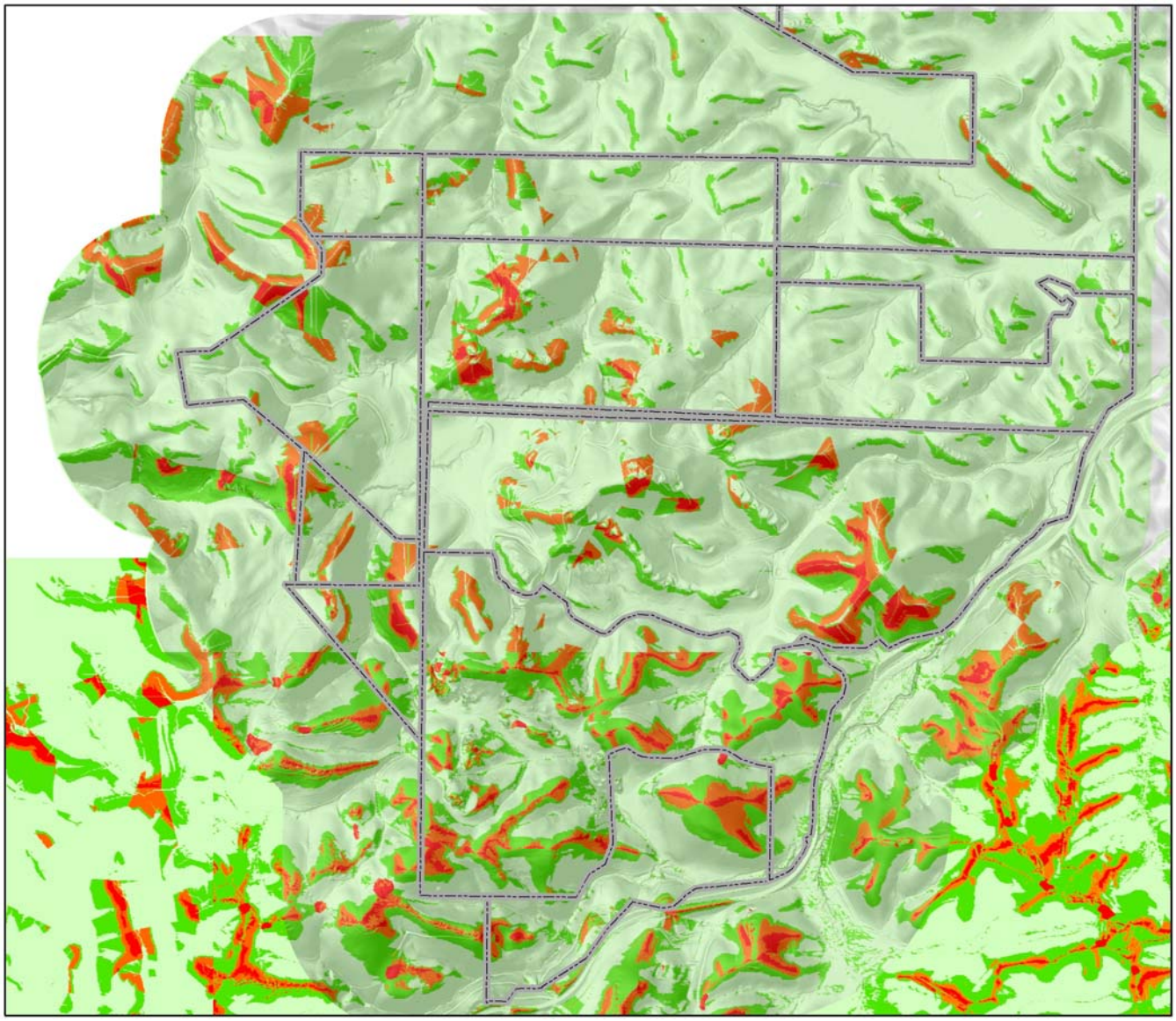

Figure 18. Projection of Fuzzy Logic likelihood surface classes of American kestrel hovering and kiting locations across entire Tres Vaqueros project area, where red corresponds with the highest likelihood of occurrence, orange corresponds with the second highest likelihood, dark green corresponds with the third highest likelihood, and light green corresponds with the least likelihood.

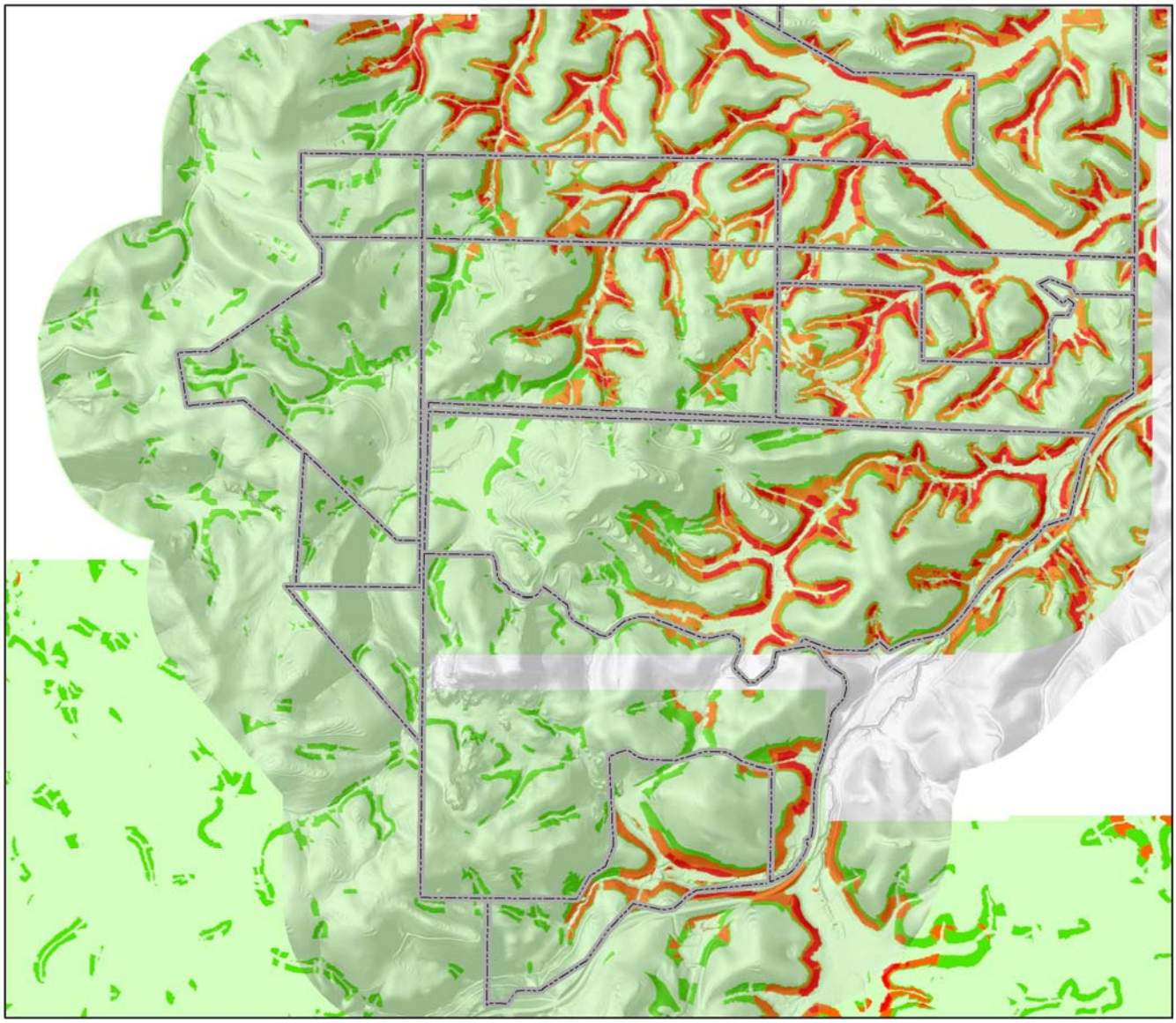

Figure 19. Projection of Fuzzy Logic likelihood surface classes of burrowing owl nest burrow locations across entire Tres Vaqueros project area, where red corresponds with the highest likelihood of occurrence, orange corresponds with the second highest likelihood, dark green corresponds with the third highest likelihood, and light green corresponds with the least likelihood.

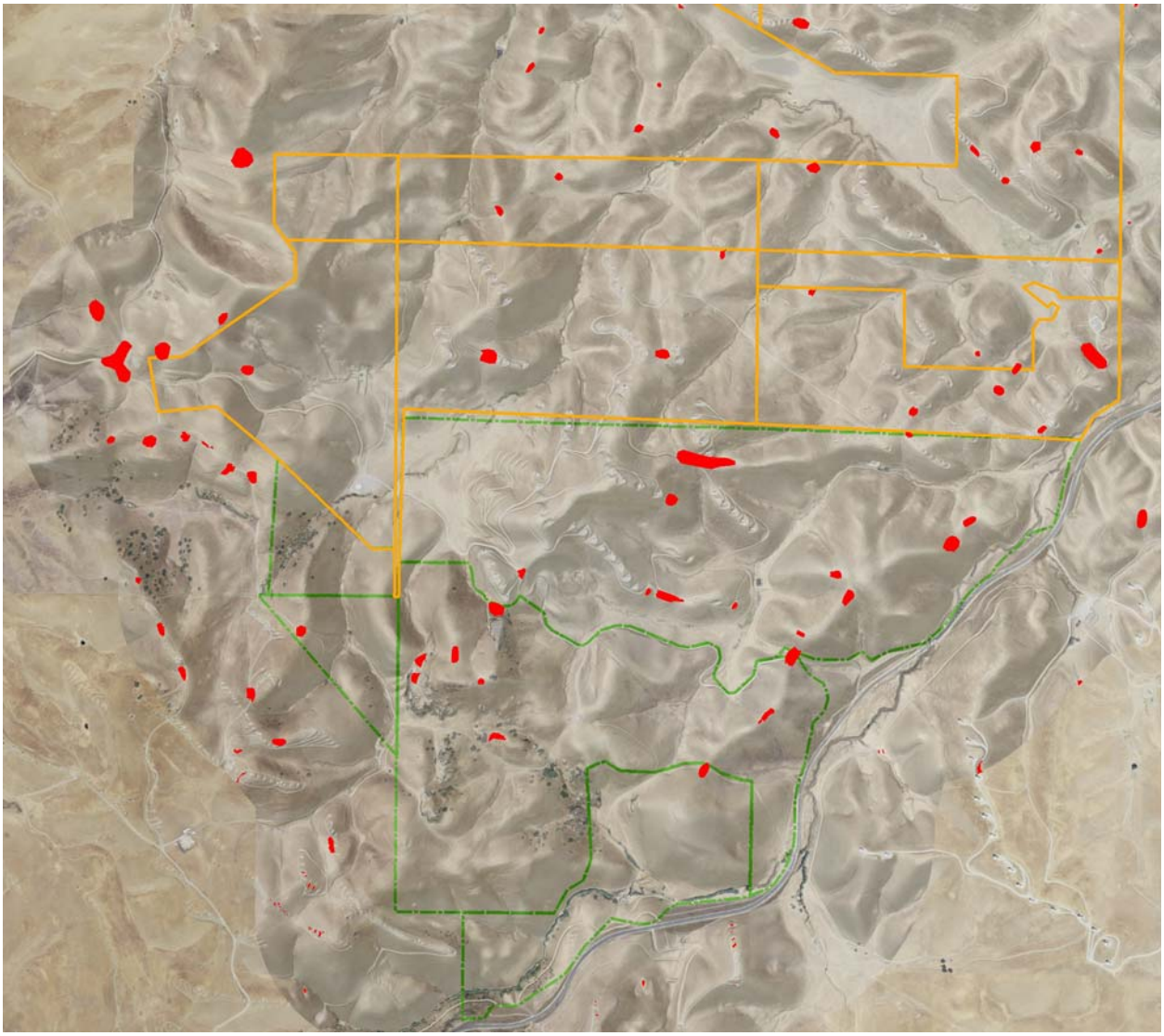

Figure 20. Hazard polygons (red) for raptors, located on ridge saddles, notches, and benches identified as relatively more likely to be used by flying raptors. Green lines denote Vasco Caves Regional Preserve and orange lines denote boundaries of properties recently acquired by East Bay Regional Park District.